NJC

Accepted Manuscript

This is an *Accepted Manuscript*, which has been through the Royal Society of Chemistry peer review process and has been accepted for publication.

Accepted Manuscripts are published online shortly after acceptance, before technical editing, formatting and proof reading. Using this free service, authors can make their results available to the community, in citable form, before we publish the edited article. We will replace this *Accepted Manuscript* with the edited and formatted *Advance Article* as soon as it is available.

You can find more information about *Accepted Manuscripts* in the Information for Authors.

Please note that technical editing may introduce minor changes to the text and/or graphics, which may alter content. The journal's standard Terms & Conditions and the Ethical guidelines still apply. In no event shall the Royal Society of Chemistry be held responsible for any errors or omissions in this *Accepted Manuscript* or any consequences arising from the use of any information it contains.

ROYAL SOCIETY OF CHEMISTRY

www.rsc.org/njc

Low Temperature Formation of Rectangular PbTe Nanocrystals and their Thermoelectric Properties

U. Nithiyanantham,[$] M. Fevzi Ozaydin,[#] Abdullah S. Tazebay,[#] and Subrata Kundu*[$]

[$]Electrochemical Materials Science (ECMS), CSIR-Central Electrochemical Research Institute (CECRI), Karaikudi-630006, Tamil Nadu, INDIA.

[#]Materials Science and Mechanical Engineering, Texas A&M University, College Station, TX 77843-3123, USA.

* To whom correspondence should be addressed, *E-mail: skundu@cecri.res.in; kundu.subrata@gmail.com*, Phone: (+ 91) 4565-241487, FAX: +91-4565-227651.

ABSTRACT

We report a low-temperature route for the successful generation of rectangular PbTe nanocrystals (NCs) within a short time under continuous heating at 80 °C. PbTe NCs are formed by the reaction of Te metal powder with Pb-acetate salt in the presence of alkaline 2,7-DHN solution in a CTAB micelle media. Two different sized rectangular PbTe NCs are synthesized just by tuning the CTAB to metal salt precursor molar ratios and controlling other reaction parameters. The optical property, thermal stability and electronic property of the PbTe NCs are studied in detail utilizing various instrumental techniques. The growth mechanism for the formation of rectangular PbTe NCs has been elaborated. Both the morphologies have been tested for their application as thermoelectric (TE) material. It was observed that both rectangular PbTe NCs can be used as thermoelectric materials and among the two morphologies, the small size rectangular PbTe NCs showed maximum TE figure of merit (ZT) value compared to large size at 475 K. The high ZT value of small size rectangular PbTe NCs compared to large size is due to its high power factor value as well as low thermal condutivity value compared to large size PbTe NCs. Other than power generation, the synthesized PbTe NCs may be further used in electrochemical biosensors, nano-optoelectronic devices and the light-use efficiency of solar devices.

Introduction

Thermoelectric (TE) technology includes power generation and electronic refrigeration. Thermoelectricity is a phenomenon of the conversion of heat into electricity directly. A typical thermoelectric device consists of p- and n- type TE materials and has many advantages, such as no moving part, no noise, contain no chlorofluorocarbon and have a long life time of reliable operation. Among this, N-type materials serves as an electron charge carriers with negative Seebeck coefficient value and p-type materials contains hole as a charge carriers with positive Seebeck coefficient value. Therefore, increasing attention has been made to TE materials during the last few years with high TE efficiency. Nevertheless, due to low efficiencies, current TE materials have found limited commercial applications. The efficiency or performance of a TE material is denoted by the dimensionless Figure of merit (ZT) where $ZT = S^2\sigma T/k$ where, S is the Seebeck coefficient, σ is the electrical conductivity, k is the thermal conductivity and T is the absolute temperature in Kelvin.[1] In order to get high TE efficiency or to increase ZT, high Seebeck coefficient, low thermal conductivity and high electrical conductivity is necessary.[2] It become a real challenge to enhance ZT value as the materials property S, σ, k will affect each other, making an optimization process necessary. Usually in TE processes, the carriers to diffuse towards the cold side and generating a thermoelectric voltage, while temperature gradient presents in the TE system. The main advantage of nanostructure TE module is lattice contribution to the thermal conductivity. In nanoscale regime heat-carrying phonons scattered by introducing a large number of grain boundaries present in nanomaterials.

Among the different types of TE materials studied so far, lead telluride (PbTe), an important group IV-VI semiconductor having a narrow band gap ~ 0.21 eV with face-centered cubic (fcc) structure[3] is one of the most commonly used materials for solid-state TE cooling and electrical power generation devices that can operate at medium temperature 450-800 K.[4] The nanoscale materials are expected to generate better TE efficiency compared to their bulk counterpart due to their large surface to volume ratio. It is reported that two-dimensional thermoelectric materials, especially nanowires, nanotubes, super-lattices have shown improved the ZT value due to quantum confinement effect, sharper density of states for enhanced thermopower and a strong phonon boundary scattering for reduced lattice thermal conductivity.[5] PbTe TE materials have been extensively studied since they exhibit high structural and chemical stability and low vapour pressure at the operating temperature range 50 °C to 600 °C. A variety

of routes have been proposed for the synthesis of PbX (X = S, Se, Te) nanomaterials including templated syntheses in mesoporous silica channels,[6] oriented attachment of nanoparticles (NPs),[7] seeded solution synthesis,[8] colloidal synthesis,[9] solvothermal,[10] hydrothermal[11] and chemical vapour transport (CVT) routes.[12] Besides, different interesting structures like NPs,[13] nanorods or nanowires,[14] nanotubes[15] have been synthesized utilizing different chemical and physical routes. Size-controlled monodispersed PbTe quantum dots were synthesized by Pan et al. using oleylamine as a capping ligand.[16] Size and shape-selective PbTe nanocrystals (NCs) were synthesized by Mokari et al. at high temperature at 250 °C.[17] Low dimension PbTe NCs were synthesized by Murphy et al. at 170 °C under inert atmosphere.[18] Hu et al. synthesized PbTe nanotubes utilizing thermal chemical reaction process.[19] Chen et al. synthesized aggregated PbTe nanomaterials utilizing gas induced reduction process at 348 K for 24 hour reaction.[20] Fardy et al. prepared PbTe chalcogenide nanowires under an inert atmosphere at high temperature.[1] Papageorgiou et al. prepared n-tupe PbTe NCs at 430 °C.[21] Sonochemical synthesis of nanocrystalline PbTe with Pb as impurity has been reported by Li et al. using Pb-acetate and Te powder as precursor by 8 hour reaction.[22] Tai et al. prepared PbTe nanowires using Te nanowire as template utilizing hydrothermal process at 180 °C for 24 hour.[23] Zhou et al. prepared flower-like PbTe nanomaterials under hydrothermal condition using Pb-acetate and Na_2TeO_3 precursor at 240 °C for 24 hour reaction.[24] Zhu et at. Prepared PbTe nanosheets using hydrothermal condition by the reaction of Pb-nitrate, Na_2TeO_3 and $NaBH_4$ at high temperature.[25] Hierarchical superstructure of lead chalcogenides were prepared by microwave assisted method with Pb-acetate and tellurium powder in ethylene glycol.[26] There are few other methods reported for the successful formation of PbTe nanomaterials utilizing various synthetic routes.[27-29] It is accepted that the presence of stabilizing agent can affect the final morphology of the nanomaterials to a great extent. Different stabilizing or capping agents had been utilized for the successful growth and formation of PbTe nanomaterials such as sodium dodecyl sulphate (SDS),[30] polyethylene glycol (PEG),[31] polyvinyl pyrrolidine (PVP)[32] and different ionic liquid etc. Most of the above methods required sophisticated precursors, high temperature, longer processing time, expensive chemicals and final products were of lacking monodispersity and resulted in mixture shapes or mixture of impurities of precursor metals with the desired nanomaterials. To the best of our knowledge, there is no report for the low temperature (60-80 °C) synthesis of rectangular PbTe NCs within a short reaction time and their morphology dependent study on TE properties.

In the present study, we highlighted for the first time, a low-temperature route for the synthesis of rectangular PbTe NCs at 80 °C within a short reaction time. PbTe NCs are synthesized by the reaction of Pb-acetate solution with Te metal powder and alkaline 2,7-dihydroxy naphthalene (2,7-DHN) solution in cetyl trimethyl ammonium bromide (CTAB) micellar media. Two different sizes of rectangular PbTe NCs are formed by tuning the surfactant to metal salt precursor molar ratios and altering the other reaction parameters. The formation and growth mechanism of rectangular PbTe NCs have been elaborated. Both the morphology has been utilized for TE applications and it was observed that rectangular PbTe NCs having small size gives better ZT value compared to large size. The synthesis process is fast, cost-effective, reproducible and may be highly beneficial for industrial scale production due to the use of fewer reagents and reduced cost via simplified low-temperature reaction.

Experimental section

Reagents.

Cetyl trimethyl ammonium bromide (CTAB, 99%), lead acetate [$Pb(CH_3COO)_2$. $2H_2O$], Te metal powder, 2,7-dihydroxynaphthalene (2,7-DHN), sodium hydroxide all are purchased from Sigma-Aldrich, India and used as received. Graphite die was used for making the pallet for TE measurements. De-ionized (DI) water was used for the entire synthesis process.

Instruments.

The synthesized CTAB-PbTe NCs were characterized with several spectroscopic techniques like UV-Vis, TEM, FE-SEM, AFM, EDS, XRD, thermal analysis and FT-IR analyses as discussed below. The UV-visible (UV-Vis) absorption spectra were recorded in a double beam UV-Vis spectrophotometer purchased from Unico (model 4802) equipped with a 1 cm quartz cuvette holder for liquid samples. The Transmission Electron Microscopy (TEM) analysis was done with JEOL-JEM 2010 and Tecnai model TEM instrument (TecnaiTM G2 F20, FEI) with an accelerating voltage of 200 KV. The Energy Dispersive X-ray Spectroscopy (EDS) analysis was done with the Field Emission Scanning Electron Microscopy (FE-SEM) instrument with a separate EDS detector connected to that instrument. The FE-SEM study was done with Zeiss ultra FE-SEM instruments. Dried PbTe powder was directly used for the characterization of X-ray diffraction (XRD), and Fourier Transform Infrared Spectroscopy (FT-IR) analyses. The

XRD analysis was done with a scanning rate of 7°/min in the 2θ range 15-80° using a Bruker X-ray powder diffractometer (XRD) with Cu K_α radiation (λ = 0.154 nm). The thermal analysis study was recorded with a thermal analyser-simultaneous TGA/DTA instrument with model name SDT Q600 and the analysis was performed in air. A hot air oven (temperature up to 1000 °C) was used to anneal the samples at a specific temperature.The FT-IR analysis was done with the model Nexus 670 (FTIR), Centaurms 10X (Microscope) having spectral Range 4,000 to 400 cm^{-1} with an MCT-B detector. Magnetic stirrer was purchased from local Balaji scientific company and used for stirring purposes during the entire work. The spark plasma sintering (SPS) process was done using a carver press with an Agilent 6680A DC power supply of 0-5V, 0-850A. For thermal diffusivity measurements a high speed Xenon lamp-pulse with pulse width of 400 μs to 600 μs having pulse energy up to15J and thermal diffusivity range up to 0.01 to 1000 mm^2/s was used in the presence of Argon atmosphere. The heat capacity measurement was done using modulated differential scanning calorimetry (MDSC) methodology using the thermal analysis instruments Q2000 modulated DSC in the temperature range of -180 °C to 725 °C with accuracy of ± 0.1 °C.

Low temperature formation of rectangular PbTe NCs.

PbTe NCs are synthesized by the reaction of Pb-acetate with Te metal powder in the presence of alkaline 2,7-DHN in CTAB micellar media. In a typical synthesis, 15 mL of 0.1 (M) CTAB was mixed with 0.6 g of Te metal powder, stirred well and heated at 60 °C initially. The solution became cement color at this stage due to Te metal powder. Then after 10 minutes, 100 mL of NaOH solution was added and stirring was continued for another 20 minutes. After that 20 mL of 2,7-DHN solution was added and the reaction temperature increases to 80 °C under continuous stirring. At this stage the cement color decreased and the solution slowly was turning to light bluish to deep bluish in color and then continuously 60 mL of Pb-acetate solution was added drop wise. After 5 minutes of the addition of Pb-acetate, a brown color precipitate became started to arise. The reaction is further continued for another 30 minutes, then stopped and cooled at a room temperature. The precipitate was settled down and washed with ethanol and water several times. After the precipitate centrifuged at 8000 rpm for 10 minutes to remove any excess surfactant or other chemicals with the reaction product. Finally, the precipitate collected and dried at 80 °C for two hours. The sample exclusively contains PbTe NCs having a smaller size of

the particles. The other morphology was also prepared just by tuning the CTAB to metal salt precursor molar ratio and the detailed concentration of all the reagents, particles size, shape, reaction time and temperature are clearly elaborated in Table 1. Scheme 1 shows the schematic formation of PbTe nanomaterials using simple wet-chemical process.

Set No.	Final conc. of CTAB (M)	Final conc. of Pb(II) Acetate solution (M)	Amount of Te metal powder (gm)	Final conc. of 2,7-DHN (M)	Final conc. of NaOH (M)	Color of the solution	Average particles size (nm)
1	7.6×10^{-5}	1.53×10^{-2}	0.6	5.12×10^{-3}	1.53	Light grey color	Side length 390 ± 20 nm, 230 ± 10 nm.
2	7.6×10^{-3}	1.53×10^{-2}	0.6	5.12×10^{-3}	1.53	Light grey color	Side length 260 ± 5 nm, 190 ± 20 nm.

Table 1: The detailed final concentrations of all the reaction parameters, time of reaction, particles size, shape etc. are summarized.

Fabrication of synthesized PbTe NCs for thermoelectric measurements.

The CTAB stabilized two different sizes rectangular PbTe NCs were used for the measurement of TE performance. The PbTe NCs were prepared as a pellet form by loading them into a graphite die and consolidating in spark plasma sintering (SPS) apparatus at different temperatures. Same amounts of each sample were taken and the graphite die was placed in the SPS chamber for sintering. In the SPS process, PbTe alloys were sintered at 300 °C under uniaxial pressure of 40 MPa for 5 min. Sintering temperature depends on the phase diagrams of PbTe. TE measurements were done below the sintering temperature because this is the safe temperature range at which the specimens would not show any premature melting by going into the mushy zone (solid + liquid). High DC current is passed between graphite electrodes and axial pressure is simultaneously applied from the beginning of the sintering cycle. Finally, after sample preparation, the materials were taken for the analysis of thermal diffusivity, electrical conductivity, Seebeck coefficient and ZT values, which has been discused in below section.

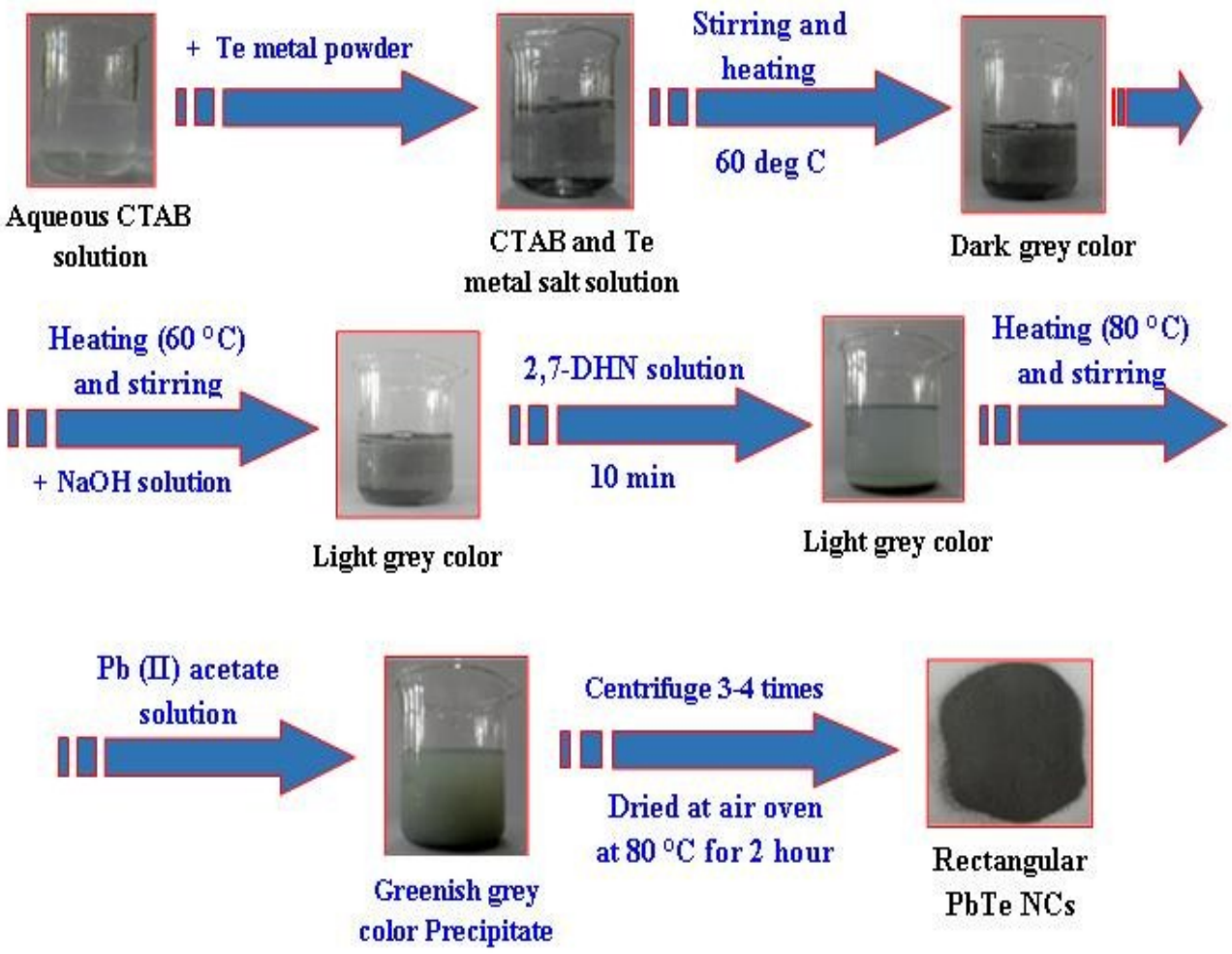

Scheme 1: The schematic presentation of the overall preparation process for the formation of PbTe NCs.

The thermal conductivity (κ) value of the PbTe NCs was evaluated from the thermal diffusivity α, heat capacity C_p, and smaple density ρ, based on the relationship $\kappa = \alpha.C_p.\rho$. Thermal diffusivity was determined by laser flash method by using flash line 3000 system and thermal diffusivity measurements was done in the temperature range from room temperature (RT) to 1000 °C. In this methodology, one side of a sample with a defined thickness was heated using a short light pulse and the resulting increase in temperature on the other side was detected via contactless infrared detector. Followed by, the bulk density of the sample was measured using standard Archimedes method. The heat capacity was measured using Modulated differential scanning calorimetry (MDSC) methodology using the TA instruments Q2000

modulated DSC in the Temperature range is -180 to 725 °C with accuracy of ± 0.1°C. In modulated DSC heat is applied simultaneously and measurement was done for how they affect the rate of heat flow. As compared to standard DSC, modulated heating rate allows the measurement of both the heat flow that responds to heating rate (Reversing signal) and the heat flow that responds to absolute temperature/time (Non-reversing signal). Heat capacity (Cp) is contained in the reversing signal.

$$\text{Rev } C_p = \frac{\text{Heat flow amplitude}}{\text{Heating rate amplitude}} \times K\,(C_p\ \text{Rev})$$

Where: K Cp Rev = Calibration constant for reversing C_p.

Preparation of samples for various characterizations.

The shape-selective CTAB-PbTe NCs were characterized using UV-Vis, TEM, EDS, XRD, XPS, thermal analyses and FT-IR studies. The PbTe NCs after successive centrifugation and drying were used for the measurement in UV-Vis spectrophotometer after dispersing in aqueous solution. The solid PbTe powder was mixed with DI water, sonicated for 30 min, and used for TEM sample preparation and other thin films preparation. The samples for TEM was prepared by placing a drop of the corresponding PbTe NCs solution onto a carbon coated Cu grid followed by slow evaporation of solvent at ambient conditions. For EDS, XRD and FT-IR analysis, glass slides were used as substrates for thin film preparation. The slides were cleaned thoroughly in acetone and sonicated for about 30 min. The cleaned substrates were covered with the PbTe NCs solution and then dried in air. After the first layer was deposited, subsequent layers were deposited by repeatedly adding more PbTe NCs solution and drying. Final samples were obtained after 4-5 times of depositions and then analyzed using the above techniques. For FE-SEM and AFM, the sample was prepared as same drop casting way over glass slide but a low concentration was used unlike XRD, FT-IR. For XPS and TGA/DTA analysis, the as prepared PbTe nano powders are directly used for the measurement. The sample preparation for thermoelectric ZT measurements has already been discussed in previous section.

Results and Discussion

UV-Vis spectroscopic analysis.

In our present route, PbTe NCs are synthesized by the reaction of Pb-acetate with Te metal powder in presence of alkaline 2,7-DHN in CTAB micellar media. In a typical synthesis, 15 mL of 0.1 (M) CTAB was mixed with 0.6 g of Te metal powder, 100 mL of NaOH solution, 20 mL of 2,7-DHN solution and 60 mL of Pb-acetate solution. Figure 1 shows the UV-Vis absorption spectra of different solution mixture for the synthesis of PbTe NCs. Curve a, in Figure 1 shows the absorption band of only aqueous CTAB solution which has no specific band in the UV-Vis region. Curve b shows the absorption band of only aqueous 2,7-DHN solution which has three distinct absorption peaks at 282 nm, 311 nm and 324 nm respectively. All these peaks appeared due to the presence of aromatic benzene rings on its structure as reported earlier. Curve c is the absorption band of only Te metal powder in water which has no distinct absorption band, but a broad hump peaking near 311 nm might be due to the formation of oxide or hydroxide compound in water. Curve d is the absorption band of Pb acetate solution which has a strong peak at 207 and a small hump at 258 nm might be due to the ligand to metal charge transfer (LMCT) spectra. Curve e shows the absorption band of the mixture of CTAB, 2,7-DHN, Te metal powder and Pb acetate salt solution which gives two small absorption bands at 291 nm, 344 nm and a strong peak at 241 nm. These peaks are shifted compared to only 2,7-DHN peak indicating that there is an interaction among them or absorption of metal ions with positively charged surfactants or any chemical reaction occurred among them. Now after the completion of reaction, the product was washed, centrifuged and re-dispersed in aqueous solution. Curve f and curve g show the absorption band of PbTe NCs for two different morphologies of small size and large size rectangular PbTe NCs respectively. In both the curve, there is no specific peak but a broad hump ranging at 350-760 nm with maximum peaking at 487 nm (small size) and 503 nm (large size) is observed. As there is no report on the electronic absorption spectra of PbTe nanomaterials, we are unable to compare our absorption data with literature. The peak maximum for both morphologies nicely matches with the change in absorption band position with particles size and shapes.

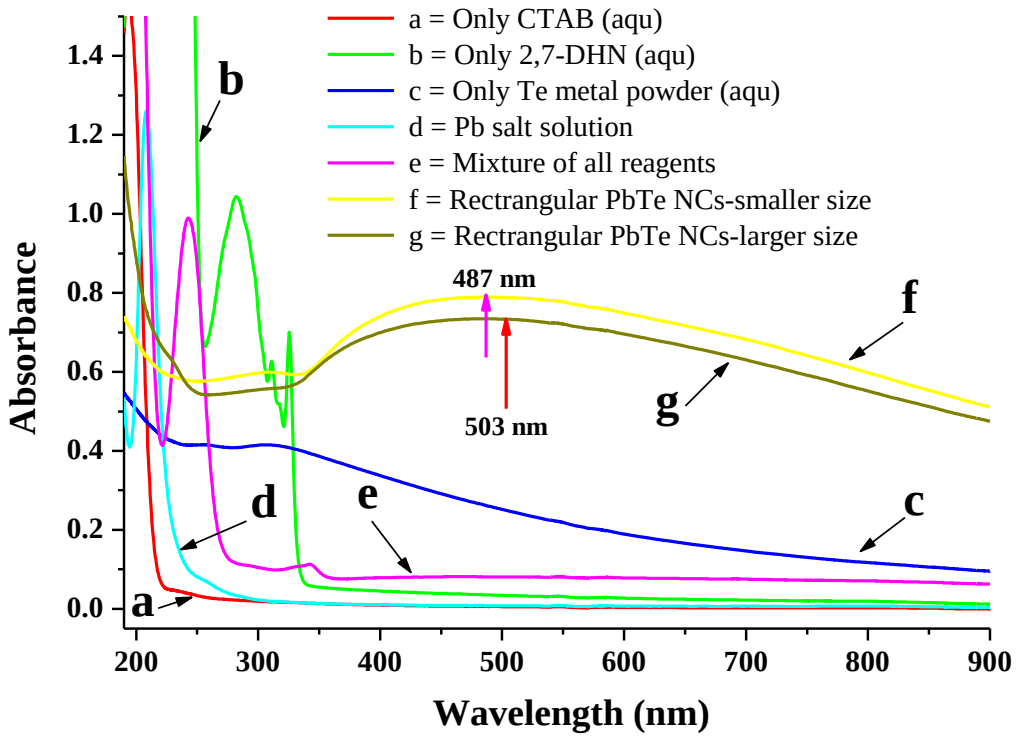

Figure 1: UV-Visible absorption spectra of different solution mixture for the synthesis of PbTe NCs. Curve (a) shows the absorption band of only CTAB solution; curve (b) shows the absorption band of only aqueous 2,7-DHN solution; curve (c) shows the absorption band of only Te metal powder in water; curve (d) shows the absorption band of Pb acetate solution; curve (e) shows the absorption band of the mixture of CTAB, 2,7-DHN, Te metal powder and Pb acetate salt solution; curve (f) and curve (g) shows the absorption band of PbTe NCs for two different morphologies of small size and large size rectangular PbTe NCs respectively.

Morphological analysis using Transmission Electron Microscopy (TEM), Field-emission Scanning Electron Microscopy (FE-SEM) studies and Energy Dispersive X-ray Spectroscopy (EDS) studies.

The transmission electron microscopy (TEM) and field-emission scanning electron microscopy (FE-SEM) images of PbTe NCs are shown in Figure 2 and Figure 3 respectively. In Figure 2, A-B shows the low and high magnified image of the rectangular PbTe NCs having smaller in size corresponds to curve f in Figure 1. Figure 2A is the low magnified picture and 2B

is the high magnified picture. From the image, the side length of the rectangular NCs was calculated. For smaller size rectangular PbTe NCs, the side length (longer side) is 260 ± 5 nm and 190 ± 20 nm (shorter side) respectively. From the image, it is clear that all the particles are formed almost uniform in size and shape. Figure 2B shows the image of single NCs. The inset of Figure 2B shows the corresponding selected area electron diffraction (SAED) pattern which speaks that the particles are crystalline in nature. A clear rectangular diffraction spots are observed from the diffraction pattern indicating the shape effect in SAED. Similar types of shape-effect SAED was observed earlier by Kundu et al. for the synthesis of triangular Au nanoprisms earlier. In Figure 2, C-D shows the low and high magnified TEM images of the rectangular PbTe NCs while the size of the particles are big corresponds to curve g in Figure 1. Figure 2C is the low magnified image where Figure 2D is the image of single NCs. From the image, the average length of the rectangular NCs are 390 ± 20 nm (longer side) and 230 ± 10 nm (shorter side) respectively. The inset of Figure 2D shows the corresponding SAED pattern which speaks that the particles are single crystalline in nature. Here also we have observed rectangular SAED pattern as discussed before. From all the images in TEM, it is cleared that each particles is separated from each other this might be due to the presence of stabilizing agent CTAB which capped the particles on their surface. Similar types of observation was noticed by others for their synthesis of metal NPs using CTAB and other different organic ligands.[33-35] Moreover, in between the particles there are some free surfactant (less contrast) is observed which we are unable to remove by repeated washing and centrifugation. Figure 3 shows the FE-SEM image of the rectangular PbTe NCs for two different morphologies that we have synthesized. Figure 3A show the high magnified FE-SEM image where size of the NCs is small. From the image, it was seen that all the particles formed the perfect rectangular shapes and they aggregate each other either due to higher concentration during sample preparation or due to slow drying process during water evaporation. The average size of the particles is calculated that matching nicely with the results obtained for the TEM analysis in Figure 2. Similarly, Figure 3B show the FE-SEM image of the rectangular PbTe NCs where the size of the particles is large and that matches nicely with the TEM results as discussed before. So by analyzing TEM and FE-SEM, we can confirm that the rectangular PbTe NCs are formed in our synthesis process. The energy dispersive X-ray spectroscopic (EDS) analysis of PbTe NCs (not shown here) consists of the different peaks correspond to the elements such as Pb, Te, C, O and Br presents to in our

synthesized product. The high intense Pb and Te peak came from the synthesized PbTe NCs while C and O peak came probably from the metal salts used or from the surfactant used during the synthesis. A small intense Br peak came from the excess CTAB which is used as a capping agent during the synthesis of rectangular PbTe NCs.

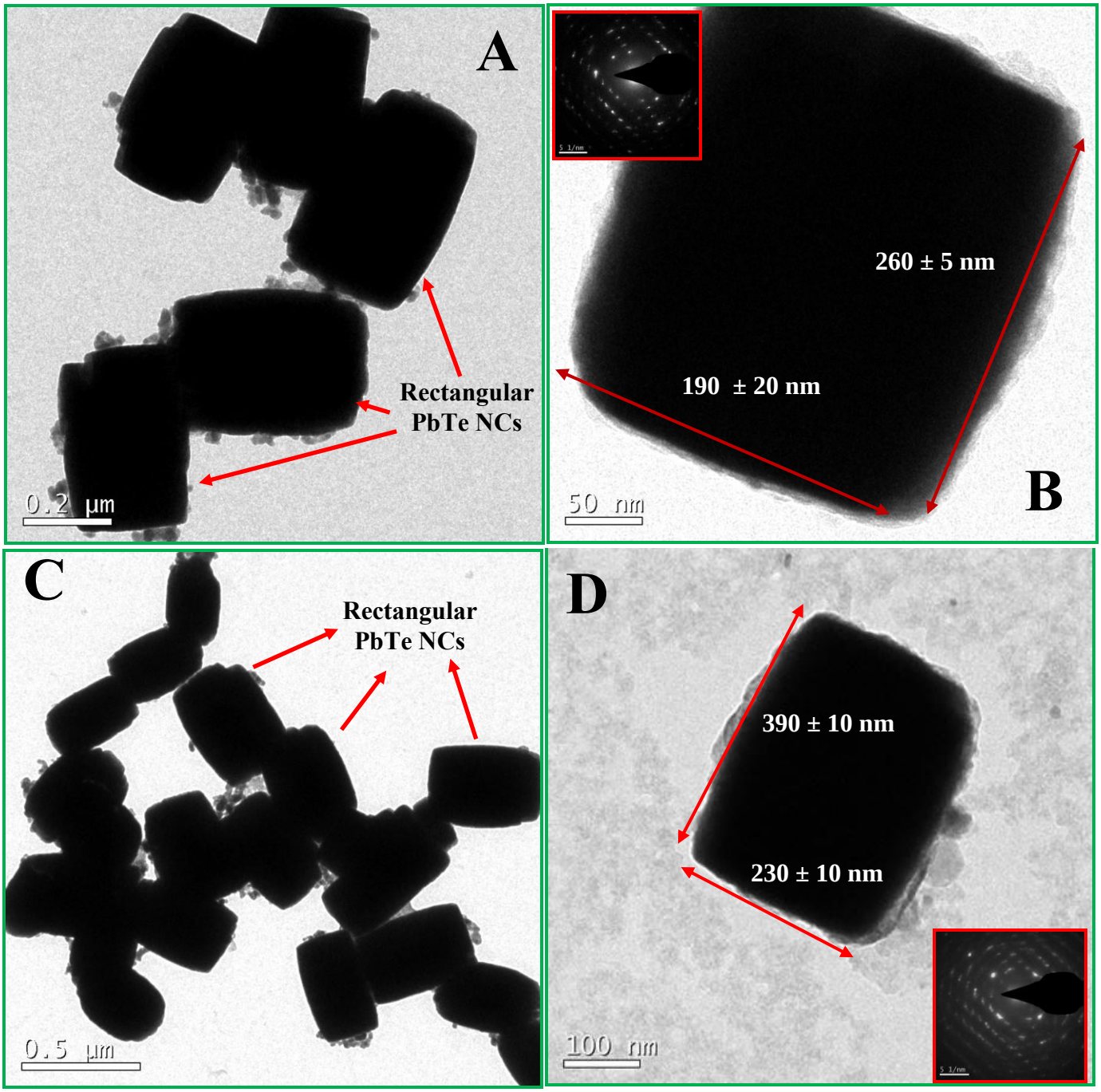

Figure 2, A-D: Transmission Electron Microscopy (TEM) image of the PbTe NCs. Figure 2, A-B shows the low and high magnified TEM image of smaller size rectangular PbTe NCs whereas Figure 2, C-D shows the larger size rectangular PbTe NCs. The inset of Figure 2B and Figure 2D shows the corresponding selected area electron diffraction (SAED) pattern.

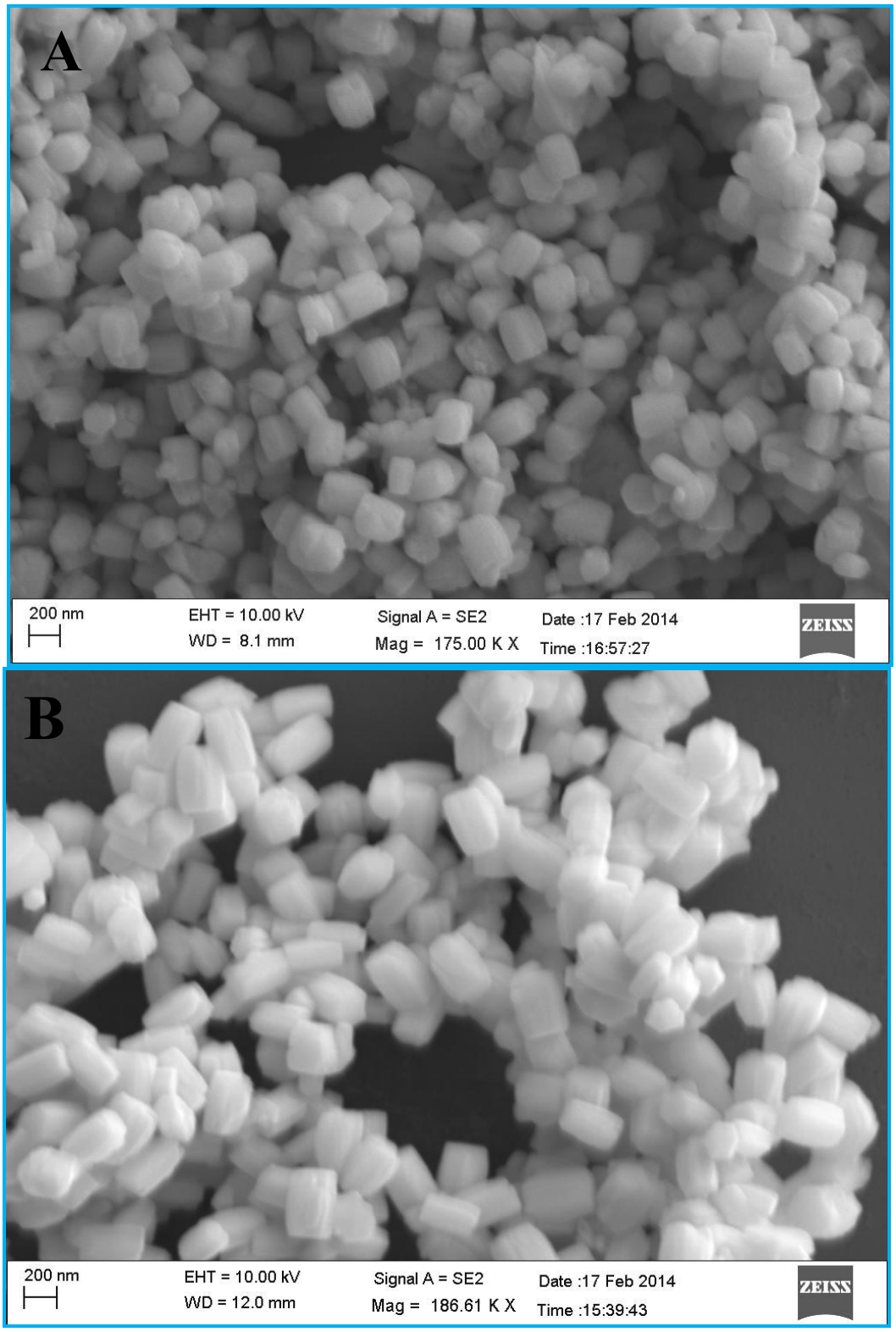

Figure 3, A-B: Field-emission scanning electron microscopy (FE-SEM) images of the rectangular PbTe NCs. Figure 3, A and B shows the high magnified FE-SEM images for smaller and larger size PbTe NCs respectively.

Study of the PbTe NCs by X-ray Diffraction (XRD) analysis.

The X-ray diffraction (XRD) pattern of the PbTe NCs is shown in Figure 4. In Figure 4, curve a and curve b indicates the XRD pattern of the small and large size PbTe NCs respectively. In both the cases, in curve a and curve b we observed exactly similar types of XRD pattern where similar peak but only the intensity changes. The XRD curves are plotted at the 2θ range 15-80 degree. The diffraction peaks are originated from the (111), (220), (200), (311), (222), (400), (331), (420) and (422) planes of PbTe NCs within the experimental error (sys: cubic, S. G.: a = 6.459 Å). All the diffraction peaks are nicely matched with joint committee for powder diffraction standard (JCPDS) file number 38-1435.[16,19] An exactly similar types of XRD pattern of cubic PbTe NCs was reported before by Pan et al.[16] and Hu et al.[19] for their synthesis of PbTe nanomaterials of different morphology. Zhu et al. synthesized PbTe nanomaterials which have face centered cubic (fcc) structure having JCPDS value 78-1905.[28]

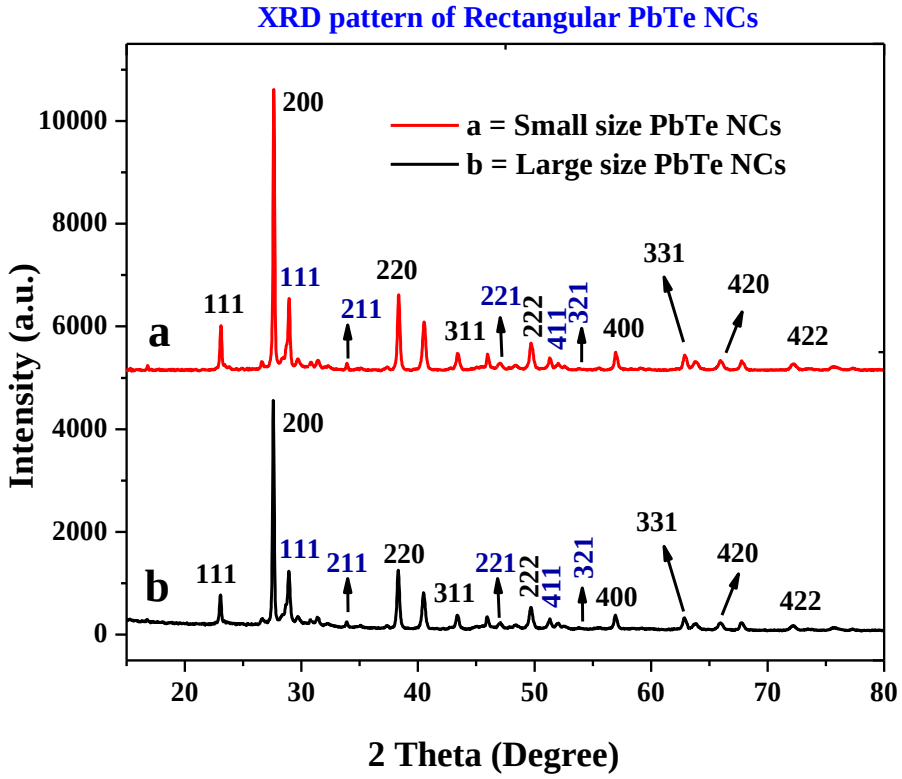

Figure 4: The X-ray diffraction (XRD) pattern of the rectangular PbTe NCs where 'a' indicates for small size PbTe NCs and 'b' indicates for larger size PbTe NCs. The planes indicated by black color is for PbTe and in blue color is for TeO_2.

In our study other than the original PbTe peaks there are few other low intense peaks were also observed that is due to the presence of impurities as TeO_2 having JCPDS file no. 52-0795. In the XRD Figure above the TeO_2 crystal planes are indicated by blue color. Now by comparing the two pattern features, the XRD pattern of the as-synthesized PbTe product exhibit that the relative intensity ratio of the strongest two peaks that are (200) and (220) is 100: 27.42 (small size) and 100 : 26.73 (large size) respectively. The ratio of this two peaks from the standard PbTe powder in the JCPDS card are 100 : 75 suggesting that the synthesized PbTe product display the preferential crystallographic orientation of the (200) compared to the standard PbTe powder.[19] The XRD pattern of the final material after spark plasma sintering (SPS) process has been recorded (not shown here) and the average crystal domain size of the two materials (before and after SPS) are compared. Before SPS, the average crystal domain size was 235 nm and 264 nm for smaller and larger size PbTe NCs whereas after SPS the average crystal domain size was 295 nm and 320 nm smaller and larger size PbTe NCs using Scherrer equation. The increase of crystal domain size is due to particles particle fusion, compacting, gain growth and increase in density while applying temperature and pressure during SPS process. Hence, we confirmed that the synthesized PbTe NCs are preferentially grown along the (200) planes compared to (220) planes and generate the rectangular shapes.

Study of the PbTe NCs by X-ray Photoelectron Spectroscopic (XPS) analysis.

Figure 5 shows the X-ray photoelectron spectroscopy (XPS) images of the PbTe NCs. In Figure 5, spectrum a denotes the survey spectrum while spectra b, c and d denotes the high resolution spectrum for Pb (4f), Te (3d) and O (1s) respectively. The survey spectrum in Figure 5a consists of the characteristic peaks for Te (3d) at 581.2 eV, O (1s) at 530.2 eV, Pb (4d) at 419.45 eV, C (1s) at 285.2 eV, Pb (4f) at 146.2 eV and O (2s) at 26.6 eV respectively. Figure 5b shows the high resolution XPS scan for Pb 4f which showed a doublet that originate due to spin-orbit coupling of Pb $4f_{5/2}$ and Pb $4f_{7/2}$ peaks. The Pb $4f_{5/2}$ peak is appeared at a binding energy of 150.1 eV while Pb $4f_{7/2}$ peak is appeared at a binding energy of 145.3 eV. All the high resolution XPS spectra are deconvoluted and fitted with background spectra to clearly understand the exact peak position. Figure 5c shows the high resolution XPS spectrum for Te 3d where the Te 3d peak shows doublet due to spin-orbit coupling of Te $3d_{3/2}$ and Te $3d_{5/2}$ peaks. The Te $3d_{3/2}$ peak is appeared at a binding energy of 586.6 eV and Te $3d_{5/2}$ peak is appeared at a binding energy of

576.2 eV. There are two other peaks also appeared at a binding energy of 592.5 eV for Te $3d_{3/2}$ (TeO_2) and 582.2 eV for Te $3d_{5/2}$ (TeO_2) respectively.

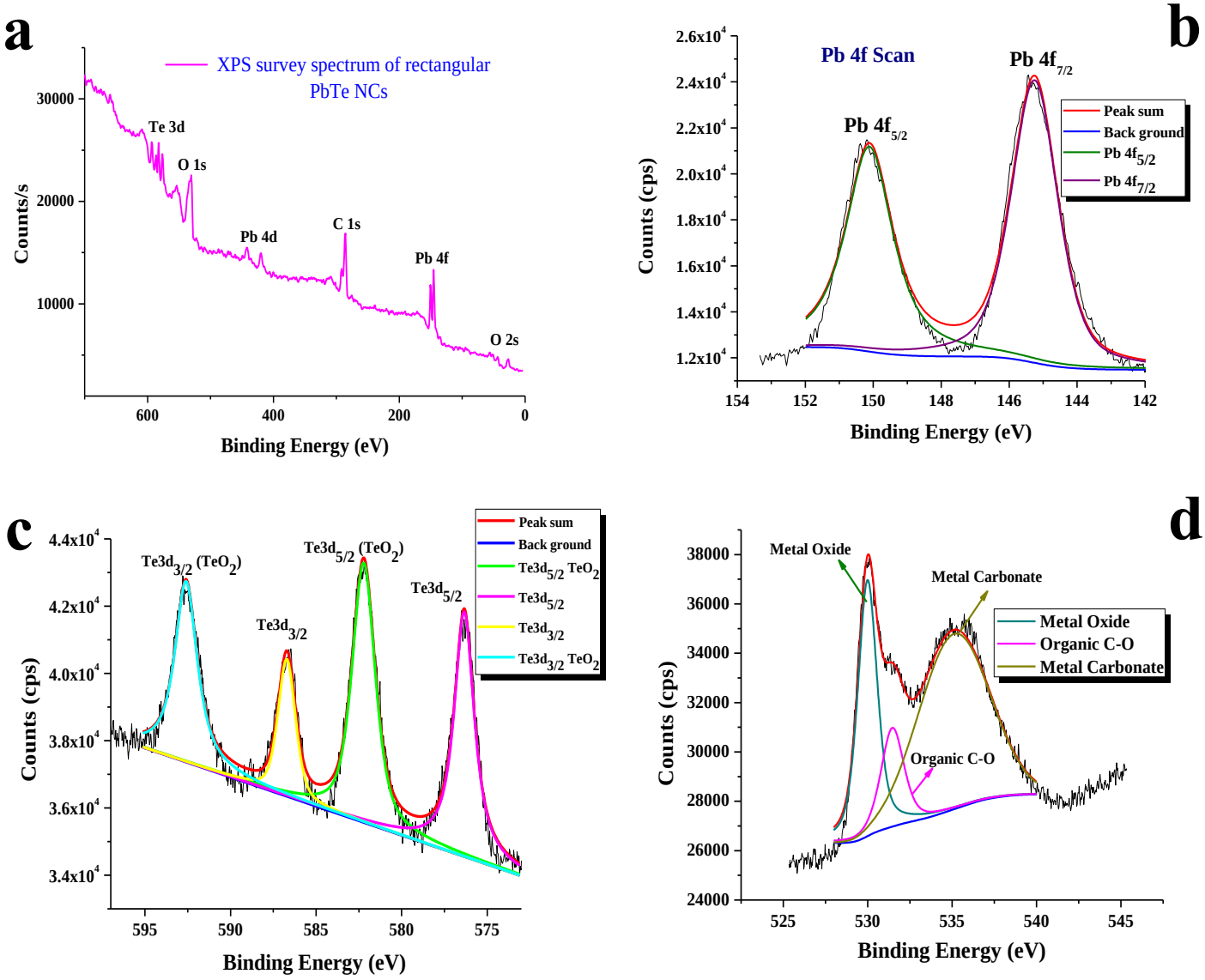

Figure 5, a-d: X-ray photoelectron spectroscopic (XPS) analysis of PbTe NCs. Figure 5 (a) shows the survey spectrum; (b) shows the high resolution scan for Pb 4f; (c) shows the high resolution scan for Te 3d peaks and (d) shows the high resolution scan for O1s XPS spectrum respectively.

Figure 5d shows the high resolution spectrum of O (1s) scan. The three different O peaks are appeared at a binding energy of 530 eV for metal oxide, 531.5 eV for organic C-O and 535.2 eV for metal carbonate respectively. From the XPS analysis we conclude that with PbTe

nanomaterials, a small amount of TeO_2 was present as impurity which further supported by XRD analysis (discussed before). A similar types of XPS spectra for PbTe were reported earliar.[33,34]

Thermal analysis.

The crystallization process of the as-prepared PbTe NCs was determined by thermo gravimetric analysis (TGA) and differential thermal analysis (DTA) using a solid as-prepared PbTe sample of 2.66 mg. the sample was heated in the air up to 1000 °C at a heating rate 10 °C per minute. In Figure 6, curve A denotes the TGA curve while curve B denotes the DTA curve. From the TGA curve, we can see that the first weight loss takes place near 109 °C might be due to the removal of moisture with the sample. The second weight loss takes place at 327 °C that is due to the removal of excess organic moieties and the excess surfactant molecules. There is another weight loss takes place near 503 °C that is most probably due to melting of excess Te metal powder in the sample. The final weight loss starts at 763 °C and continues until the end which might be due to the melting of PbTe. Curve B shows the DTA curve where there is an endothermic peak appeared at 323 °C and there is a strong exotherm appeared at 470 °C.

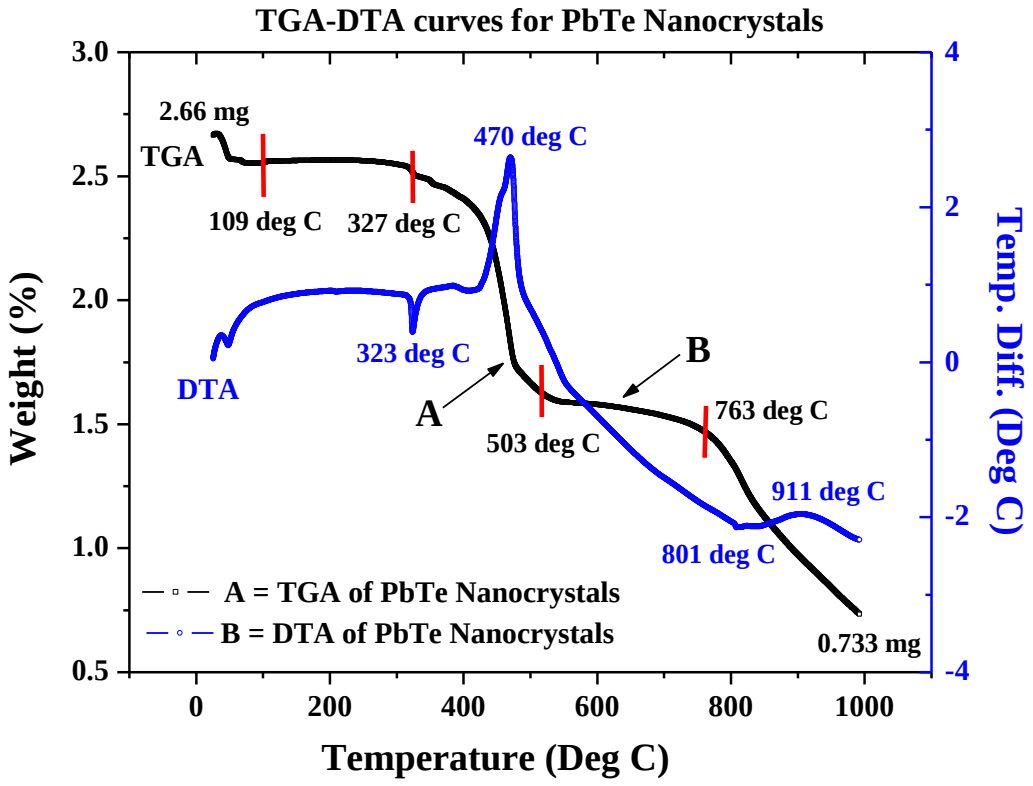

Figure 6: Thermal analysis of as-synthesized PbTe NCs where curve A denotes the TGA curve while curve B denotes the DTA curve.

This is probably due to evaporation of excess CTAB or excess metal salt precursor. The final exotherm near 910 °C is due to melting of the synthesized PbTe NCs. A similar type of thermoelectric analysis was reported earlier by others.[21,35] From the above thermal analysis we can see that we have started our reaction taking 2.66 mg of sample and heating it up to 1000 °C and the amount of sample remaining is 0.733 mg. Hence the % of weight loss in this process is 72.44 %.

FT-IR analysis.

The FT-IR analysis of only CTAB and CTAB capped PbTe NCs are shown in Figure 7. We plot both CTAB and CTAB capped PbTe spectra together which not only supports the presence of surfactant on the PbTe NCs surface but also provide the nature of interaction taking place among them. We checked that both the morphology of rectangular PbTe NCs gives similar types of FT-IR pattern. So here we plot the FT-IR spectrum of large size rectangular PbTe NCs. As the transmittance (%) value of CTAB capped PbTe NCs is less compared to only CTAB, the intensity of the peaks for CTAB-PbTe is less compared to only CTAB when plotting them together. In case of only CTAB sample, a small peak at 3470 cm^{-1} is appeared which is due to -OH stretching originated from water molecule or adsorbed moisture during analysis. A broad peak at 3331 cm^{-1} is due to well-known –N-H stretching vibration for pure CTAB molecule. There are three strong and intense peaks appeared for only CTAB sample at 3012 cm^{-1}, 2918 cm^{-1} and 2847 cm^{-1} which is due to –C-H stretching and anti-stretching vibration in $–CH_2$ group of the CTAB molecule. The 3331 cm^{-1} peak is not observed in the case of CTAB bound PbTe sample rather than several low intense peak appeared in the region 3536-3170 cm^{-1} indicates the interaction of CTAB with PbTe NCs. The –C-H stretching and bending peaks are also shifted in case of CTAB-PbTe sample to 2926 cm^{-1} and 2846 cm^{-1} indicating the interaction of the surfactant with PbTe NCs. In case of only CTAB sample, there are few other peaks are appeared in the region 1350-1800 cm^{-1} peaking at 1795 cm^{-1}, 1628 cm^{-1}, 1470 cm^{-1} and 1391 cm^{-1} might be originated due to –C-N stretching, $-CH_2$ scissoring mode of vibration and –OH bending mode of water around the bound head group. All these peaks are not visible or shifted in case of CTAB bound PbTe sample indicates the interaction among them. In case of CTAB-PbTe sample, the peaks are appeared at 1739 cm^{-1} and 1397 cm^{-1} respectively. Now at lower wavenumber region at 600-1000 cm^{-1} specifically at 955 cm^{-1}, 906 cm^{-1} and 724 cm^{-1} peaks are appeared due to

stretching vibration of tertiary amine [$RN(CH_3)_3^+$], -CH_2 rocking which is not at all visible in case of CTAB bound PbTe sample. Most of the peaks for CTAB and CTAB capped PbTe NCs are described above matched with earlier reports for CTAB capped metal and metal oxide nanostructures. So after analyzing the FT-IR data it is cleared that CTAB is capped the PbTe NCs and stabilized them after the synthesis. A similar type of ligand stabilized PbTe NCs was reported earlier.[21, 36] The specific FT-IR peaks of CTAB (reported value)[37] and the FT-IR peaks for CTAB that observed experimentally and the corresponding peak assignments are summarized in Table 2.

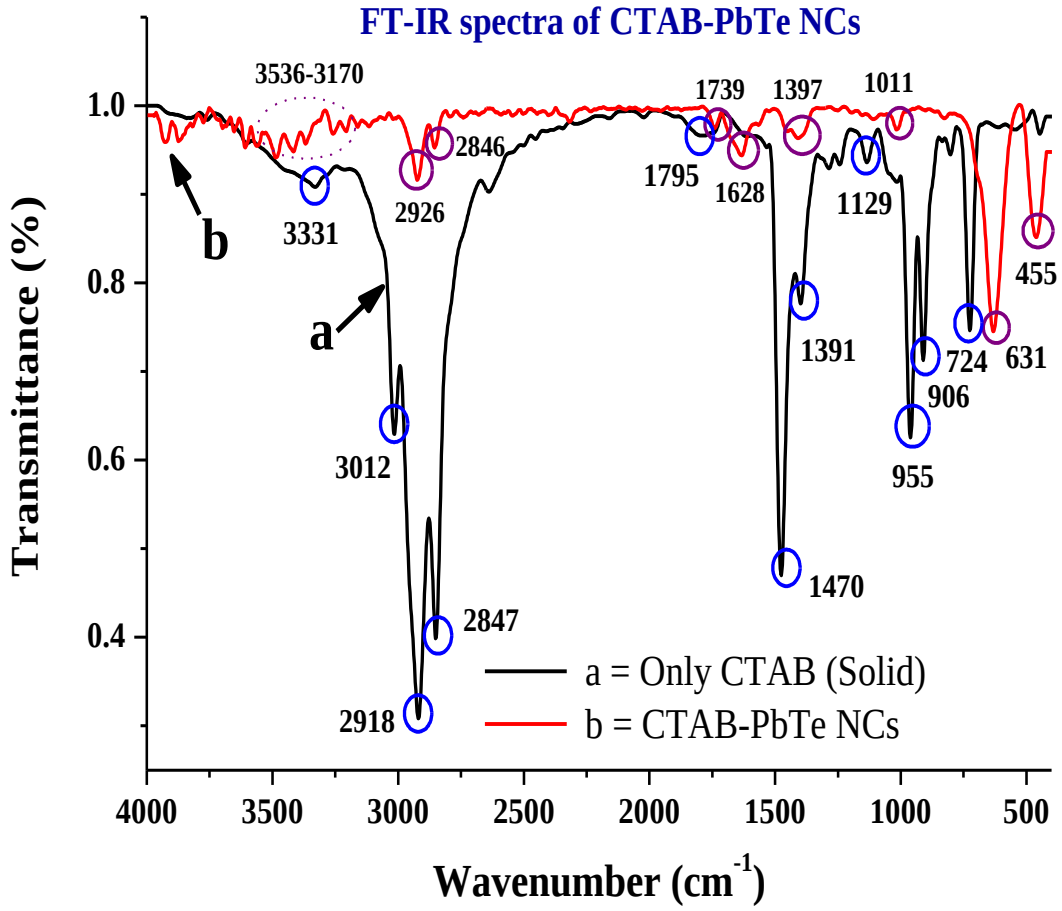

Figure 7: The Fourier-transform infrared (FT-IR) spectra of only CTAB (curve a) and CTAB bound PbTe NCs (curve b) in the wavenumber range 400-4000 cm^{-1}.

FT-IR bands – cetyl trimethyl ammonium bromide (CTAB)-Experimental and Reported values		
FT-IR bands (cm^{-1}) (experimentally observed)	**FT-IR frequency range (cm^{-1}) (reported value)**	**Absorbing bonds/vibration types**
3331	3330	–N-H stretching vibration
3012	2959, 2870	$-CH_3-$ anti-symmetrical and symmetrical stretching
2918, 2847	2916, 2828	$-(CH_2)-$ anti-symmetrical and symmetrical stretching
1391	1376	$-CH_3-$ symmetric deformation
1129, 1253, 1284	1300-1000 (1041,1151,1265)	$-(CH_2)-$ out-plane swinging
1034	1040	Symmetric stretching vibration C-N bonds
906, 955, 1470	908, 961, 1472	Tertiary Amine $[RN(CH_3)_3^+]$
724	720, 728	$-(CH_2)-$ in-plane swinging
Reference: Huang, L.; Chen, X.; Li, Q. *J. Mater. Chem.* **2001**, 11, 610.		

Table 2: The details about the different FT-IR bands reported for CTAB, the experimentally observed bands of CTAB and their corresponding band assignments.

Mechanism for the formation of rectangular PbTe NCs.

Rectangular PbTe NCs are formed by the reaction of Te metal powder with lead acetate solution in the presence of alkaline 2,7-DHN in CTAB micellar media at low-temperature by heating at 80 °C. Two different sizes but same rectangular morphologies were formed just tuning the CTAB to metal salt precursor molar ratio. In our study, we conducted some control experiment to check the role of all the reagents used. We have seen that by keeping all the reaction parameter fixed but just in absence of CTAB, PbTe nanomaterials are formed but have no specific size and shape rather they get agglomerated after formation due to absence of any specific stabilizing agent as observed from TEM analysis (image not shown here). On the other

hand in the absence of alkaline 2,7-DHN, no reaction takes place as there is no reducing agent in the solution for the reduction of Te metal powder to generate Te^{2-} ions. So a proper concentration of all the reagents is extremely necessary for the formation of specific shaped PbTe NCs. In our experiment, we checked the pH of the different solution mixtures during synthesis. The pH of only Te metal powder aqueous solution is 5.38, pH of Pb-acetate solution is 6.04, pH of only alkaline 2,7-DHN solution is 13.20, pH of only CTAB solution is 5.66 and pH of the mixture of all the reagents containing Te metal powder, Pb acetate, 2,7-DHN, NaOH and CTAB is 11.65. So our overall reaction takes place at a basic pH. After the formation of two different morphology, we checked the pH of an aqueous dispersion of PbTe NCs which are 8.23 and 8.54 for small and large size rectangular PbTe NCs respectively. In our study we did the experiment at a low-temperature ~ 80 °C, so we believe only ionic process takes place. Zhu et al.[28] reported earlier that in the presence of sodium borohydride as reducing agent while the reaction takes place at a high-temperature, both ionic and atomic processes takes place for the formation of PbTe NCs. In their reaction, they add the entire precursor at the same time and autoclave at a higher temperature so both atomic and ionic processes can contribute for the formation of PbTe NCs. Moreover, Zhu et al. also referred that when the same reaction they carried out at low temperature (~ 70 °C), they did not observe PbTe but they got PbO, tellurium oxide and Te even if the reaction time increases to 24 hours.[28] Hence we confirmed that in our present study at low temperature, sequential addition of reagents only contribute the ionic process for the generation of PbTe NCs. The possible chemical reactions that take place in our study are:

$$\text{Te metal powder} + \text{CTAB} \xrightarrow{60\ ^{o}\text{C}} \text{Te@ CTAB}$$

$$3Te + 6OH^{-} \xrightarrow{60\ ^{o}\text{C}} 2Te^{-2} + TeO_3^{-2} + 3H_2O$$

$$3TeO_3^{-2} + 3C_{10}H_8O_2 \xrightarrow{60\ ^{o}\text{C}} 2Te^{-2} + TeO_2 + 3C_{10}H_8O_2^{-2} + H_2O$$

$$Te^{-2} + Pb^{+2} \xrightarrow{80\ ^{o}\text{C}} \text{PbTe@CTAB}$$

So in the proposed reaction, we believed that completely ionic process was involved to generate PbTe and a small amount of impurity as tellurium oxide was present in the final product which confirmed by the XPS and XRD analysis. Zhu et al.[28] mentioned that at lower temperature once you add all reagents at once, there is possibility of partial lead reduced from Pb^{+2} and did not completely reacts with Te and were easy to be oxidized to PbO during the filtering and drying process. So in our reaction alkaline 2,7-DHN acts as mild reducing agent which convert TeO_3^{-2} to Te^{-2} and CTAB acts as shape-directing[35] and capping agent for the generation of PbTe NCs. It was already reported previously that compound having hydroxyl group in their structure like TX-100,[38] Ascorbic acid,[39] 2-naphthol,[35] poly vinyl alcohol[40] can act as reducing agents for the reduction of metal ions to metal NPs. Kundu et al. have also observed before that 2,7-DHN in alkaline condition can reduce metal salts of Au,[41] Ag,[42] Pd,[43] Os[44] to their corresponding metal NPs. Even it is also reported that de-oxyribonucleic acid (DNA) having hydroxyl group on its sugar analogue can be used to reduce metal ions to generate DNA templated metal NPs.[45-47] So in our present process, once Te metal reduced by alkaline 2,7-DHN to form Te^{-2} and when the lead salt added in the reaction mixture, they react each other immediately and generate PbTe nuclei. Once the PbTe nuclei are formed, they grow indiscriminately accumulating more Te^{-2} ions and creating a void space surrounding the full grown particles. The PbTe nuclei are formed close to interface and favor crystallization in a preferential direction. With increasing time, the formation of PbTe nuclei is reduced and finally slow crystallization process takes place and all the PbTe nuclei are converted to PbTe particles as a rectangular shape. As the solution already contains the CTAB surfactant, the micelle gets adsorbed on the particular facet of the PbTe crystal and directs the 3D growth of the evolved NPs to give the desired rectangular shape. It is reported in literature that the formation of specific shape depends upon two key factors; one is the faceting tendency of the stabilizing agent and other is the growth kinetics that is rate of supply of PbTe (0) to the different crystallographic planes.[48] The surfactant CTAB adsorb onto the surfaces of these crystalline particles and slow down the growth rate of different crystal facets. We observed that in both the CTAB concentrations rectangular PbTe particles are formed although the size of the particles was smaller at higher CTAB concentration while the size of the particles larger at low CTAB concentration. It is reported that when the growth rate of (111) plans and (100) plans are almost same, mostly nanocubes are formed but once the growth rate is slightly more or less any of the planes, rectangular morphology can be formed. Hence in our case

we confirmed that the growth rate of the two facets are not completely equal and results in rectangular shaped particles. Xia's group have also reported before that while the growth rate is predominant in either (100) or (111) direction, mostly anisotropic shapes like tetra-pods, octa-pods are formed.[49,50] Murphy et al.[18] have also reported that high surface energy {111} face growth in the <111> direction is faster relative to that of the large surface energy {100} face growth in the <100> direction and favors the growth of {100} faces more and generate cubic morphology. In our case, at a high CTAB concentration, the growth rate in both the crystal faces is somehow restricted and results in smaller size rectangular PbTe NCs while in comparatively lower CTAB concentration the growth in both faces is more and results in large size rectangular PbTe NCs. The evolved rectangular PbTe NCs are well separated to each other is due to the fact that CTAB surfactant adsorbed on the particle surface might form a capping shell to generate regular inter-particle spacing and these prevents the rectangles from random agglomeration.[51] At this point, the exact bonding geometry and the nature of the selective interaction between crystallographic plans are still not fully clear and further study is necessary which will be conducted in near future. Now, taking the two different morphologies of the PbTe NCs, we studied their applications in thermoelectric power generation study as discussed below.

Thermoelectric applications of Rectangular PbTe NCs.

In our present method we synthesized two different size of rectangular shape PbTe (NCs) using wet-chemical route. The wet-chemical route easily produced nanoscale dimension and used to reduce the thermal component via phonon scattering and decoupling electrical and thermal conductivities.[52] Eventhough, there are few reports are available based on the synthesis of PbTe nanomaterials, we focused here about the size effect of the nanomaterials over the TE behaviour. The synthesized PbTe NCs were analyzed for thermal diffusivity, electrical conductivity Seebeck coefficient and finally conclude with the ZT value. Theoretical and experimental report of different TE materials says that high phonon anharmonicity are the most important to design the high TE material.[53-58]

In the present analysis, we compared the TE properties of two different sizes rectangular shaped PbTe NCs. For TE measurement, all the samples were gone for SPS consolidation at 300° C under 400 MPa pressure for 5 minutes and the relative density of the samples were about 98.5%. Figure 8A shows the electrical conductivity measurment of small (a) and large (b) size

rectangular PbTe NCs with respect to temperature. The small size PbTe NCs shows typical semiconductor behavior in the temperature range between 300-380K because while increasing the temperature, the electrical condutivity is also increasing. After 380K, it show metalic behaviour, because while increasing the temperature the condutivity was decreasing. From the small size of the rectangular NCs in the range of 380 K may be there is a structure phase transition occurred, it also obtained from earlier report and it shows around 410 K for the Ag_2Te alloy structure of Ag_2Te changes from β-Ag_2Te to α-Ag_2Te, due to much decrease in carrier concentration.[59] However, small size rectangular PbTe NCs has a noticeable flattenning which begins at 400K and shows degenerate semiconductor behavior at high temperatures due to decrease in electron-electron and electron-phonon scattering conductivity. Finally, at a temperature of 480K, the small size rectangular PbTe NCs show high electircal condutivity behavior. The large size rectangular PbTe NCs intially showed metallic behaviour but after certain temperature, it changes to semiconduting in nature. At high temperatures as the carrier concentration increases, the Seebeck values decrease as shown in Figure 8b. As we will note from the Seebeck coefficient versus Temperature graphs that small (a) and large (b) size samples show degenerate (highly doped) behavior, which means as the temperature increases, the Seebeck values was also increases.

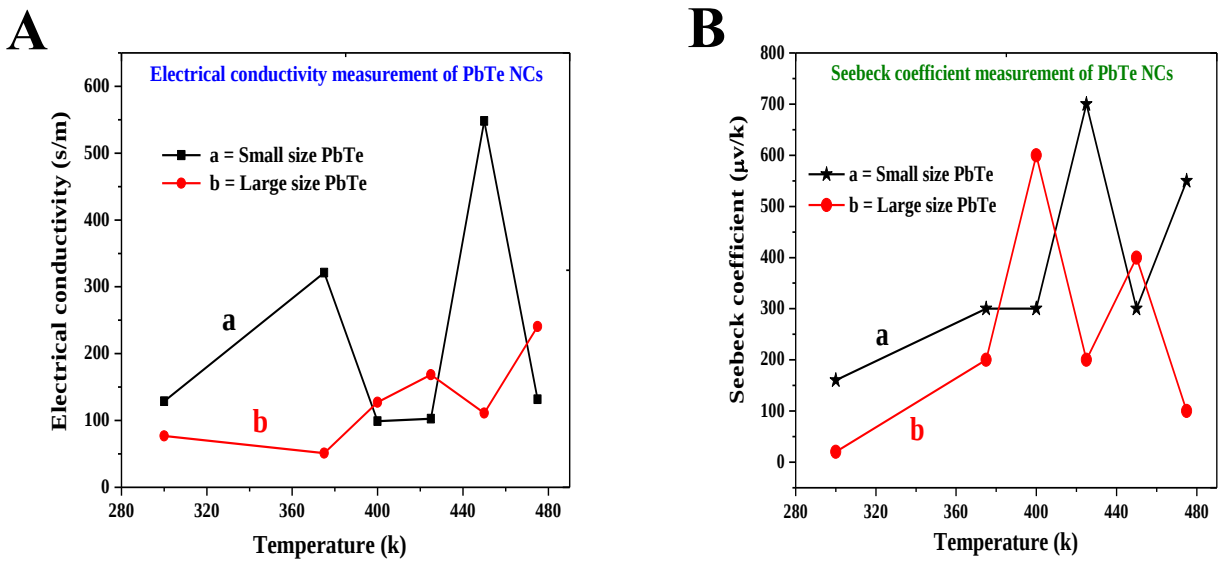

Figure 8, A-B: Thermoelectric behavior of the synthesized small (a) and large (b) size rectangular PbTe NCs. (A) Electrical conductivity measurement and (B) Seebeck coefficient analysis with change in temperature.

However, both of the samples show typical intrinsic semiconductor behavior results in decrease of Seebeck coefficient at high temperatures. The properties of Seebeck coefficient is also depends on the electrical conductivity of the materials. From the curve, we can see there is sudden increase and decrease takes place at the range between ~ 370-460K in both sample which may be due to structural phase transition as it observed by earlier report.[59] The high values Seebeck coefficient obtained at high temperature due to the well-known contribution of the two valence bands present in PbTe.[57]

The change in thermal conductivity values as a function of temperature is shown in Figure 9A. The thermal behavior of both small (a) and large (b) size rectangular PbTe NCs are gradually decreasing with increasing temperature. All the κ values decrease for both sizes PbTe system indicating the Umklapp scattering (phonon-phonon scattering) at high temperatures. At a temperature of 475K, the small and large size PbTe NCs showed nearly same thermal condutivity around 1.3 W m^{-1} K^{-1}. In case of nanomaterial, while grain sizes smaller than 5 μm, then the lattice thermal conductivity is reduced by ca. 28% compared to their bulk ones. Particles with sizes in the range of 30–200 nm, having crystallites of 5–15 nm size shows boundary scattering of phonons and reduces the thermal conductivity by ca. 46% which leads to reduced electron mobility and enhance the increase in ZT.[60] Generally the low lattice thermal conductivity obtained due to the phonons scattered by the impurity present in the atoms.[61]

Figure 9B shows the temperature dependent ZT values of two different sizes PbTe NCs. The small size (a) rectangular PbTe NCs achieved the maximum ZT value of ~ 0.1 at 475K while the larger size (b) showed the maximum ZT value ~ 0.015 at 400K. We compared the values at different temperatures because the larger size give much less ZT value at 475K. The ZT value of small size PbTe NCs shows a linear increament with increasing temperature. From the electrical conductivity mesurment, it was already observed that the small size rectangular PbTe NCs showed higher electrical conductivity compared to large size PbTe NCs (Figure 7a). The seebeck coefficient value reduce at ~ 440K, indicates the high condutivity behaviour of the sample. The low dimension nanostructure materials shows phonon-glass/electron-crystal (PGEC) that leads to achieve high TE performance.[52, 62, 63] Hence all the above analysis indicates that the small size PbTe NCs having high power factor value as well as low thermal condutivity value compared to large size PbTe NCs which in-turn show high ZT value compared to large size rectangular PbTe NCs.

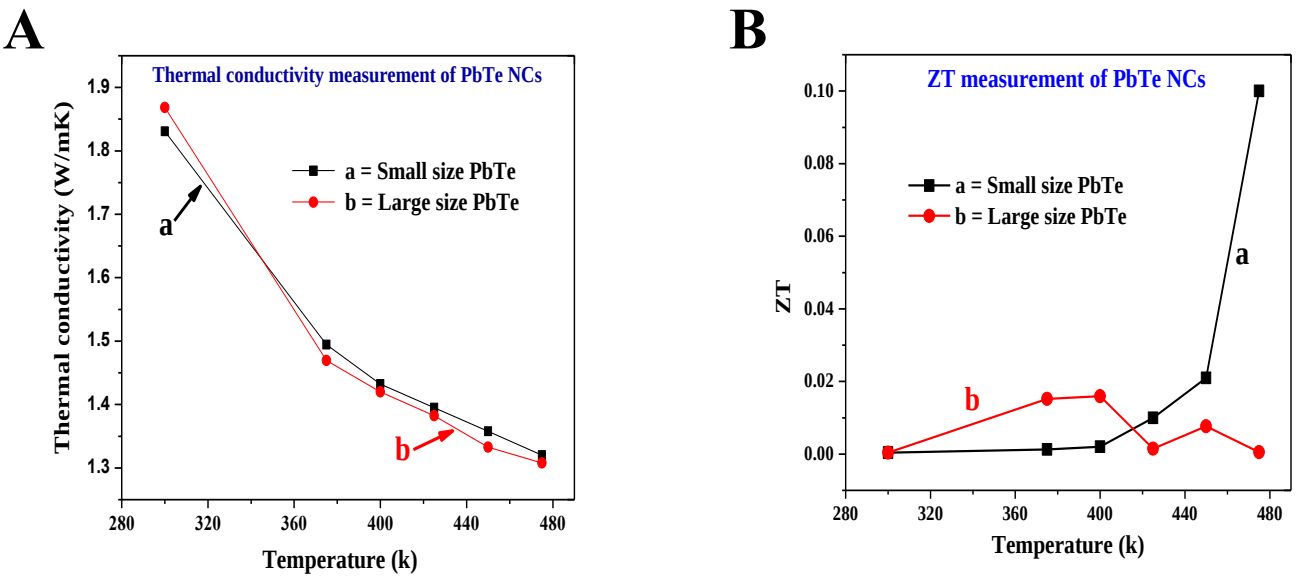

Figure 9, A-B: Thermoelectric behavior of the synthesized small (a) and large (b) size rectangular PbTe NCs. (A) Thermal conductivity measurement; (B) Figure of merit (ZT) value with change in temperature.

Conclusion:

In conclusion, we report for the first time, a low-temperature route for the successful generation of rectangular PbTe nanocrystals within a short time under heating at 80 °C. PbTe nanocrystals are formed by the reaction of Te metal powder with Pb-acetate salt in the presence of alkaline 2,7-dihydroxy naphthalene solution in a cetyl trimethyl ammonium bromide micelle media. Two different sizes rectangular PbTe nanocrystals are formed just by tuning the cetyl trimethyl ammonium bromide to metal salt precursor molar ratios and controlling other reaction parameters. The average size of the small size rectangular nanocrystals is 260 ± 5 nm (longer side) and 190 ± 20 nm (shorter side) and the large size rectangular nanocrystals is 390 ± 20 nm (longer side) and 230 ± 10 nm (shorter side) respectively. The optical property, thermal stability and electronic property of the PbTe nanocrystals are studied in detail utilizing various instrumental techniques. The growth mechanism for the formation of rectangular PbTe nanocrystals has been elaborated in details. Finally, both the morphologies have been used for their application as thermoelectric material. It was observed that both rectangular PbTe nanocrystals can be used as thermoelectric materials and among the two morphologies, small

size rectangular PbTe nanocrystals giving better thermoeletric figure of merit value compare to large size at 475 K. The achievement of the higher efficiency in case of smaller size rectangular PbTe nanocrystals due to its higher power factor value and low the thermal conducting properties. In futuristic, we will try to improve the observed efficiency to a great extent by controlling the nanomaterial morphology by introducing impurity or dopants with the synthesized material.

Acknowledgement: S. Kundu wishes to acknowledge Dr. Vijayamohanan K. Pillai, Director, and Dr. M. Jayachandran, HOD, ECMS division, CSIR-CECRI for their continuous support and encouragement. U. Nithiyanantham wishes to thank CSIR-CECRI for research-intern fellowship. Critical discussion with Prof. H. Liang at TAMU, Ede Sivasankara Rao and S. Anantharaj, CSIR-CECRI is greatly acknowledged. The institute start up funding (Project number IHP 0067, DU No 5, old number OLP-0067), support from the Central Instrumental Facility (CIF) and help from Mr. A. Rathishkumar (TEM in-charge), Mr. J. Kennedy (XPS in-charge), Mr. V. Prabu (FE-SEM in-charge, CIF), CSIR-CECRI, Karaikudi are greatly appreciated.

References.

(1) M. Fardy, A. I.Hochbaum, J.Goldberger, M. M. Zhang and P. Yang, *Adv. Mater.*, 2007, **19**, 3047.

(2) H. J. Goldsmid, *CRC Handbook of Thermoelectrics, ed*. By D.M. Rowe (Boca Raton, FL: CRC Press, 2006).

(3) M. Baleva and E.Mateeva, *Phys. Rev. B.*, 1994, **50**, 8893.

(4) G. L. Benneu, in *CRC Handbook of Thermoelectrics* (Ed.: D. M. Rowe), CRC, New York, 1995, p. 515.

(5) L. D. Hicks and M. S. Dresselhaus, *Phys. Rev. B*, 1993, **47**, 12727.

(6) F. Gao, Q. Lu, X. Liu, Y. Yan and D. Zhao, *Nano Lett*., 2001, **1**, 743.

(7) K.-S .Cho, D. V.Talapin, W. Gaschler and C.B. Murray, *J. Am. Chem. So*.,2005, **127**, 7140.

(8) K. L. Hull, J. W.Grebinski, T. H. Kosel and M. Kuno, *Chem. Mater.*, 2005, **17**, 4416.

(9) E. Lifshitz, M. Bashouti, M. V.Kloper, A.Kigel, M. S. Eisen and S. Berger, *Nano Lett*., 2003, **3**, 857.

(10) C. Zhang, Z. Kang, E. Shen, E. Wang, L. Gao, F. Luo, C. Tian, C. Wang, Y. Lan, J. Li and X. Cao, *J. Phys. Chem. B*, 2006, **110**, 184.

(11) L. Zhang, J. C. Yu, M. Mo, L. Wu, K. W. Kwong and Q. Li, *Small*, 2005, **1**, 349.

(12) J.-P. Ge, J. Wang, H.-X. Zhang, X. Wang, Q. Peng and Y.-D Li, *Chem. Eur. J*.,2005, **11**, 1889.

(13) H. Q. Liu, F. X.Hao, J.Guo, Y.J. Gu, Q.K. He and H. Z. Cui, Proc. 2012 Int. Conf. on 3M-NANO, Xi'an, China, August–September 2012, IEEE, 382–384.

(14) H. Li, K. F.Cai, J. L Yin, H. F. Wang, and X. L. Li, Y. Y. Wang and C. W. J. Zhou, *J. Nanosci. Nanotech*., 2010, **10**, 5831.

(15) L. Ao, L. J. Wang andW. Z. Wang, *Micro Nano Lett*., 2012, **7**, 621.

(16) Y. Pan, H. Bai, L. Pan, Y. Li, M. C.Tamargo, M. Soheld and J. R. Lombardiab, *J. Mater. Chem*., 2012, **22**, 23593.

(17) T. Mokari, M. Zhang and P. Yang, *J. Am. Chem. Soc*., 2007, **129**, 9864.

(18) J. E. Murphy, M. C. Beard, A. G. Norman, S. P.Ahrenkiel, J. C. Johnson, P. Yu, O. IMicic, R. J.Ellingson and A. J. Nozik, *J. Am. Chem. Soc*.,2006, **128**, 3241.

(19) J. Hu, Z. Chen, H. Jiang, Y. Sun, Y. Bandoc, and D. Golberg, *J. Mater. Chem*., 2009, **19**, 3063.

(20) S. Chen, K. F. Cai and F. Y. Li, *Mater. Res. Innovations*, 2014, **18**, S4-97.

(21) C. Papageorgiou, J. Giapintzakis and T. Kyratsi, *J. Electronic Mater*., 2013, **42**, 1911.

(22) J. –F. Li, W. –S. Liu, L. –D. Zhao and M. Zhou, *NPG Asia Mater*., 2010, **2**, 152.

(23) G. A. Tai, B. Zhou and W. L. Guo, *J. Phys. Chem. C*, 2008, **112**, 11314.

(24) N. Zhou, G. Chen, X. Yang and X. Zhang, *J. Phys. Chem. Solids*, 2012, **73**,280.

(25) T. J. Zhu, X. Chen, X. Y. Meng, X. B. Zhao and J. He, *Cryst. Growth Des*., 2010, 10,3727.

(26) H. Cao, Q. Gong, X. Qian, and H. Wang, J. Zai, and Z. Zhu, *Cryst. Growth Des*., 2007, **7**,425.

(27) Q. Li, Y. Ding, M. Shao, J. Wu, G. Yu and Y. Qian, *Mater. Res. Bull*, 2003, **38**,539.

(28) T. J. Zhu, Y. Q. Liu and X. B. Zhao, *Mater. Res. Bul*, 2008, **43**, 2850.

(29) H. Du, C. Chen, R. Krishan, T. D. Krauss, J. M. Harbold, F. W. Wise, M. G. Thomas and J.Silcox, *Nano Lett*., 2002, **2**,1321.

(30) F. Soofivand, F. Mohandes and M. Salavati-Niasari, *Micro Nano Lett*., 2012, **7**, 283.

(31) D. Zhang, H. Fu, L. Shi, C. Pan, Q. Li, Y. Chu and W. Yu, *Inorg. Chem*., 2007, **46**, 2446.

(32) F. Mohandes and M. Salavati-Niasari, *Ultrason. Sonochem*., 2013, **20**,354.

(33) R. Jin, G. Chen, J. Pei, J. Sun and Q. Wang, *Cryst. Eng. Comm*., 2012, **14**, 4461.

(34) W. Zhao, P. Y. Ge, J. J. Xu and H. Y. Chen, *Langmuir*, 2007, **23**, 8597.

(35) S. Kundu, S. Panigrahi, A. Pal, S. Basu, S. Praharaj, S. K. Ghosh and T. Pal, *Nanotechnology*, 2007, **18**, 75712.

(36) S. AhMadian-Fard-Fini, M. Salavati-Niasari and F. Mohandes, *Bull. Mater. Sci*., 2014, **37**, 753.

(37) L. Huang, X. Chen and Q. Li, *J. Mater. Chem*., 2001, **11**, 610.

(38) S. Kundu, K. Wang and H. Liang, *J. Phys. Chem. C*, 2009, **113**, 134.

(39) A. Pal and T. Pal, *J. Raman Spectrosc*., 1999, **30**, 199.

(40) S. Kundu, D. Huitink, K. Wang and H. Liang, *J. Colloid Interface Sci*.,2010, **344**, 334.

(41) S. Kundu, L. Peng and H. Liang, *Inorg. Chem*., 2008, **47**, 6344.

(42) S. Kundu, K. Wang and H. Liang, *J. Phys. Chem. C*, 2009, **113**, 134.

(43) S. Kundu, K. Wang, S. Lau and H. Liang, *J. Nanopart. Res*., 2010, **12**, 2799.

(44) S. R. Ede, U. Nithiyanantham and S. Kundu, *Phys. Chem. Chem. Phys*., 2014, **16**, 22723.

(45) S. Kundu, *Phys. Chem. Chem. Phys*., 2013, **15**, 14107.

(46) D. Majumdar, A. Singha, P. K. Mondal and S.Kundu, *ACS Appl. Mater. Interfaces*, 2013, **5**, 7798.

(47) U. Nithiyanantham, S. R. Ede and S. Kundu, *J. Mater. Chem. C*, 2014, **2**, 3782.

(48) J. M. Petroski, Z. L. Wang, T. C. Green and M. A. El-Sayed, *J. Phys. Chem.* B,1998, **102**, 3316.

(49) T. Herricks, J. Chen and Y. Xia, *Nano Lett*., 2004, **4**, 2367.

(50) B. Lim, X. Lu, M. Jiang, P. H. C. Camargo, E. C. Cho, E. P. Lee and Y. Xia, *Nano Lett*.,2008, **8**, 4043.

(51) C. B. Murray, C .R. Kagan and M. G. Bawendi, *Annu. Rev. Mater. Sci*., 2000, **30**,545.

(52) C. Kim, D. H. Kim, H. Kim and J. S. Chung, *ACS Appl. Mater. Interfaces.*, 2012, **4**, 2949.

(53) H. Zhang and D. V. Talapin, *Angew. Chem. Int. Ed*., 2014, **53**, 9126.

(54) H. Liu, X. Shi, F. Xu, L. Zhang, W. Zhang, L. Chen, Q. Li, C. Uher, T. Day and G. J. Snyder, *Nat. Mater*., 2012, **11**, 422.

(55) C. Wood, *Rep. Prog. Phys*., 1988, **51**, 459.

(56) G. H. Dong, Y. J. Zhu and Li-Dong Chen, *J. Mater. Chem*., 2010, **20**, 1976.

(57) K. Biswas, J. He, I. D. Blum, C. I. Wu, T. P. Hogan, D. N. Seidman, V. P. Dravid, M. G. Kanatzidis, *Nature*,2012,**489**, 414.

(58) L. D. Zhao, S. H. Lo, Y. Zhang, H. Sun,G. Tan, C. Uher, C. Wolverton, V. P. Dravid and M. G. Kanatzidis, *Nature*, 2014, **508**, 373.

(59) J. Pei, G. Chen, D. Jia, Y. Yu, J. Sun, H. Xu and Z. Qiu, *New J. Chem.*, 2014, **38**, 59.

(60) P. Vaqueiro and A. V. Powell, *J. Mater. Chem*., 2010, **20**, 9577.

(61) P. Zhu, Y. Imai, Y. Isoda, Y. Shinohara, X. Jia and G. Zou, *Materials Transactions*, 2005, **46**, 1810.

(62) K. Kurosaki, T. Matsuda, M. Uno, S. Kobayashi and S. J. Yamanaka, *Alloys Compd*., 2001, **319**, 271.

(63) S. Paschen, V. Pacheco, A. Bentien, A. Sanchez, W. C. Cabrera, M. Baenitz, B. B. Iversen, Y. Grin and F. Steglich, *Physica B*, 2003, **328**, 39.

Figure Captions:

Figure 1. UV-Visible absorption spectra of different solution mixture for the synthesis of PbTe NCs. Curve (a) shows the absorption band of only CTAB solution; curve (b) shows the absorption band of only aqueous 2,7-DHN solution; curve (c) shows the absorption band of only Te metal powder in water; curve (d) shows the absorption band of Pb acetate solution; curve (e) shows the absorption band of the mixture of CTAB, 2,7-DHN, Te metal powder and Pb acetate salt solution; curve (f) and curve (g) shows the absorption band of PbTe NCs for two different morphologies of small size and large size rectangular PbTe NCs respectively.

Figure 2. Transmission Electron Microscopy (TEM) image of the PbTe NCs. Figure 2, A-B shows the low and high magnified TEM image of smaller size rectangular PbTe NCs whereas Figure 2, C-D shows the larger size rectangular PbTe NCs. The inset of Figure 2B and Figure 2D shows the corresponding selected area electron diffraction (SAED) pattern.

Figure 3. Field-emission scanning electron microscopy (FE-SEM) images of the rectangular PbTe NCs. Figure 3, A and B shows the high magnified FE-SEM images for smaller size and larger size PbTe NCs respectively.

Figure 4. The X-ray diffraction (XRD) pattern of the rectangular PbTe NCs where 'a' indicates for small size PbTe NCs and 'b' indicates for larger size PbTe NCs.

Figure 5. X-ray photoelectron spectroscopic (XPS) analysis of PbTe NCs. Figure 5 (a) shows the survey spectrum; (b) shows the high resolution scan for Pb 4f; (c) shows the high resolution scan for Te 3d peaks and (d) shows the high resolution scan for O1s XPS spectrum respectively.

Figure 6. Thermal analysis of as-synthesized PbTe NCs where curve A denotes the TGA curve while curve B denotes the DTA curve.

Figure 7. The Fourier-transform infrared (FT-IR) spectra of only CTAB (curve a) and CTAB bound PbTe NCs (curve b) in the wavenumber range 400-4000 cm^{-1}.

Figure 8. Thermoelectric behavior of the synthesized small (a) and large (b) size rectangular PbTe NCs. (A) Electrical conductivity measurement and (B) Seebeck coefficient analysis with change in temperature.

Figure 9. Thermoelectric behavior of the synthesized small (a) and large (b) size rectangular PbTe NCs. (A) Thermal conductivity measurement; (B) Figure of merit (ZT) value with change in temperature.

Table 1: The detailed final concentrations of all the reaction parameters, time of reaction, particles size, shape etc. are summarized.

Table 2: The details about the different FT-IR bands reported for CTAB, the experimentally bands we observed and their corresponding bond assignments.

Scheme 1. The schematic presentation of the overall preparation process for the formation of PbTe NCs.

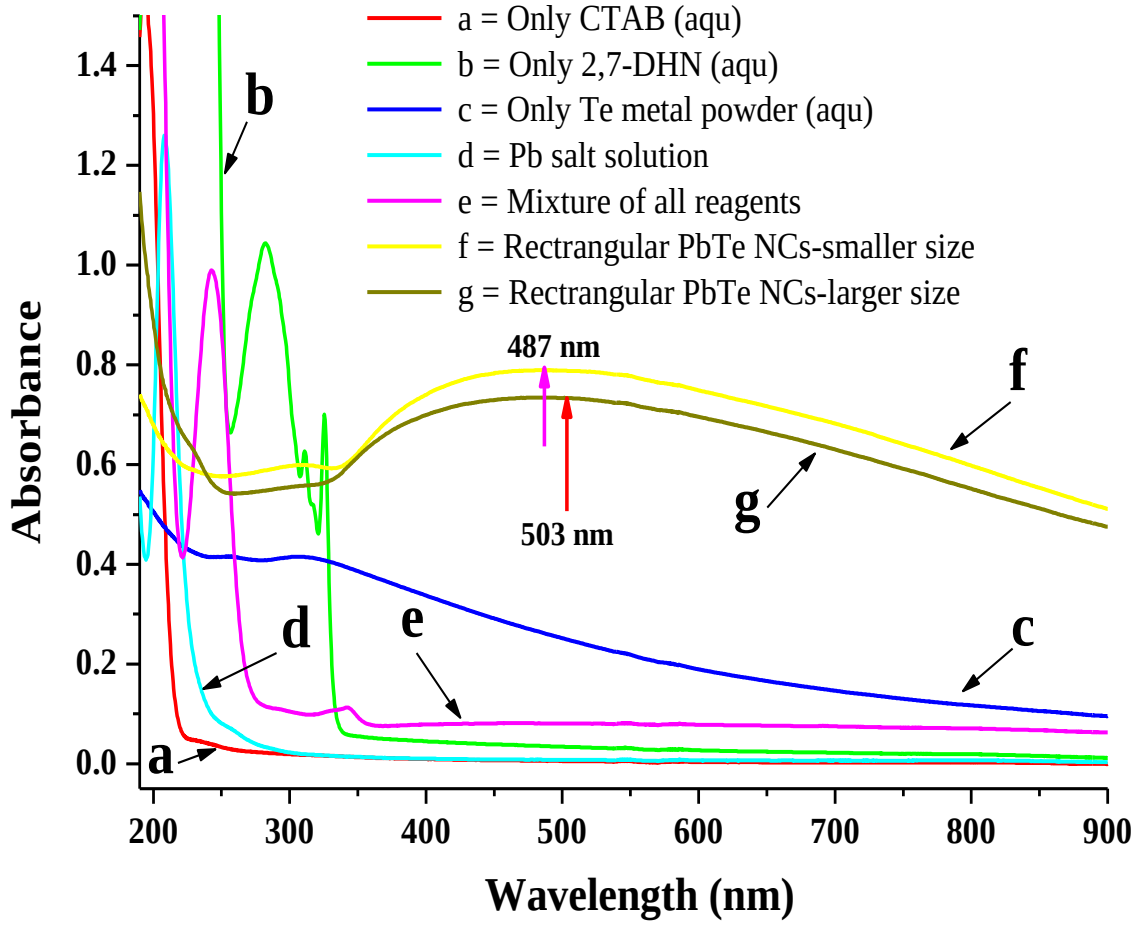

Figure 1

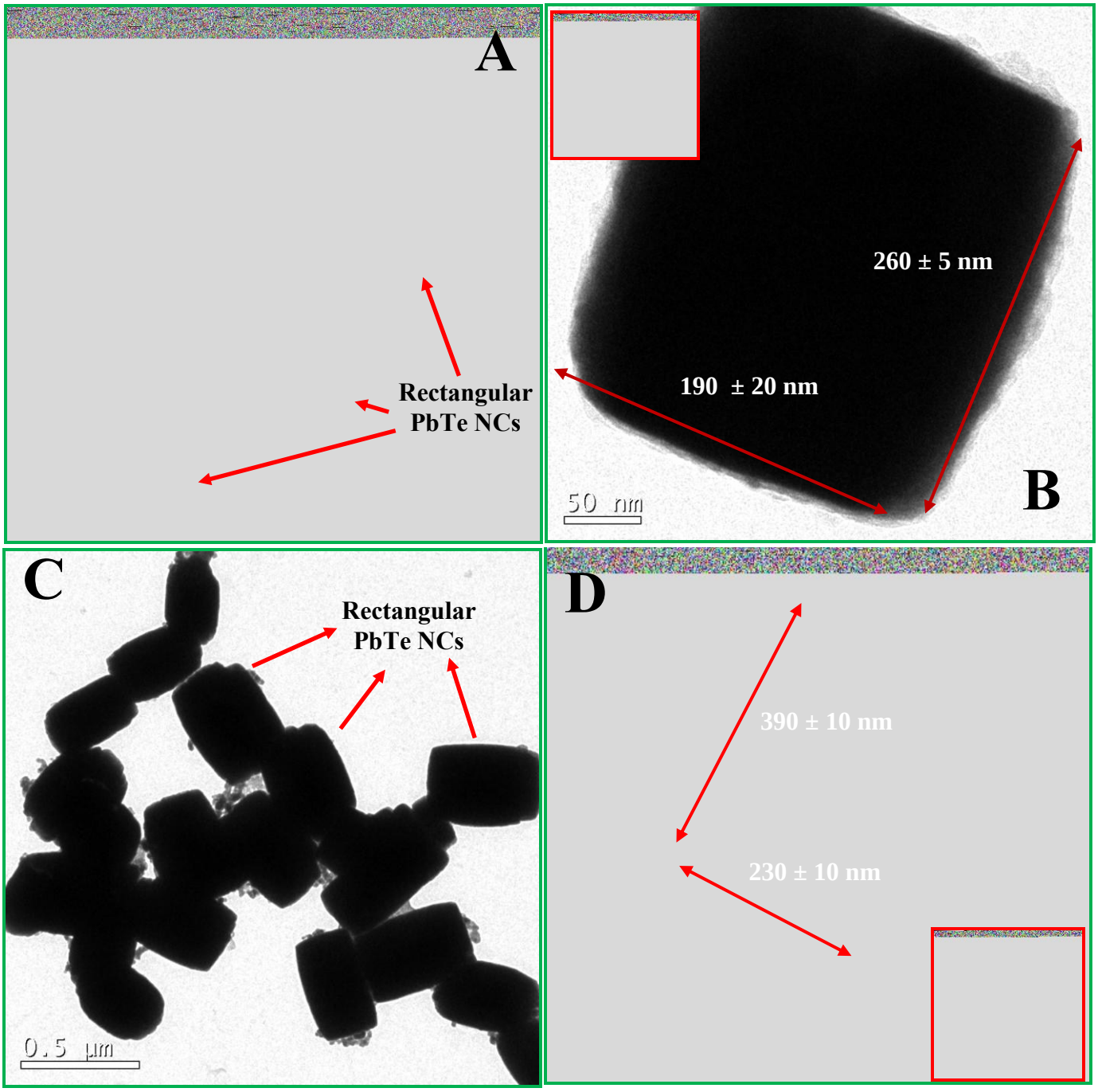

Figure 2, A-D

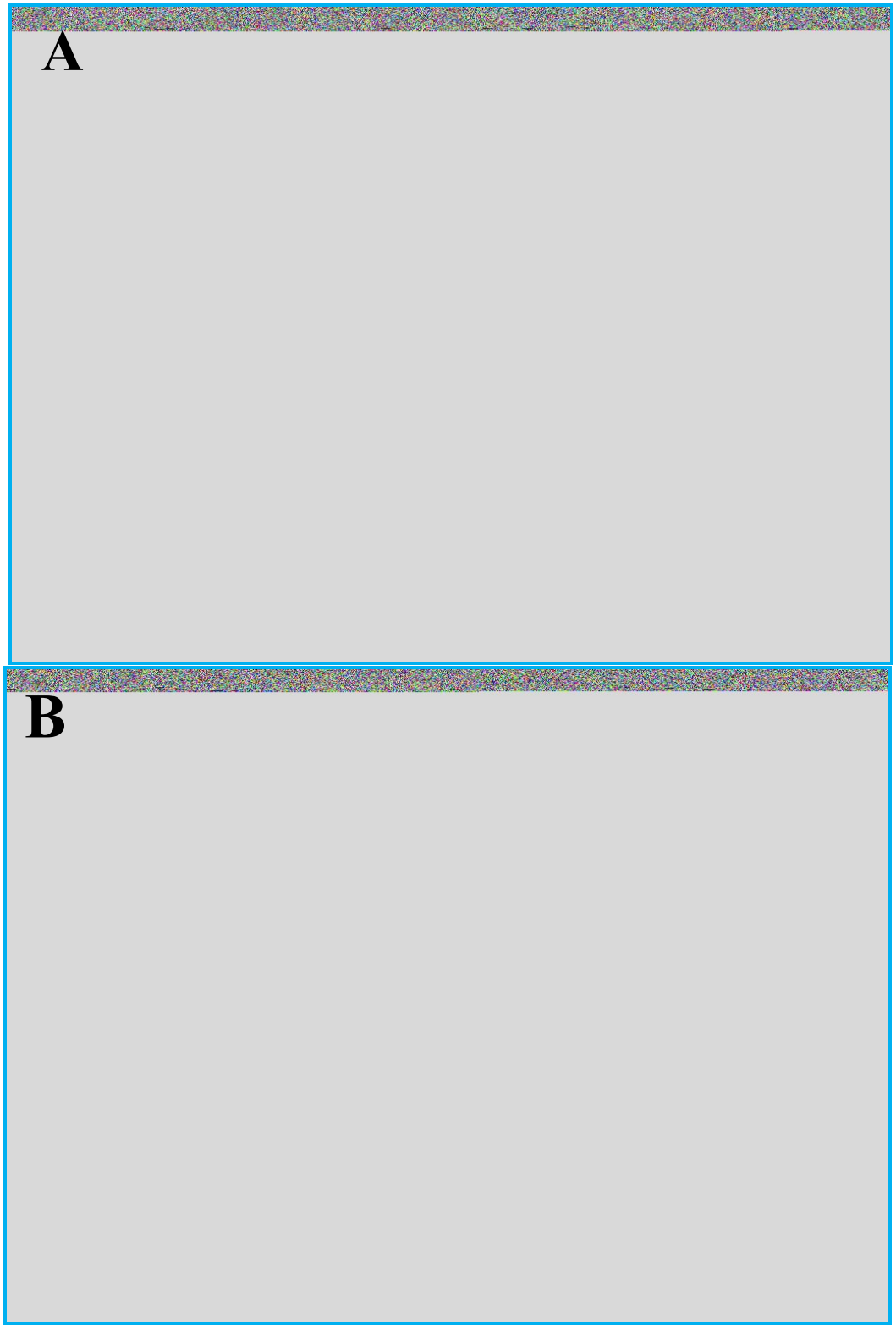

Figure 3, A-B

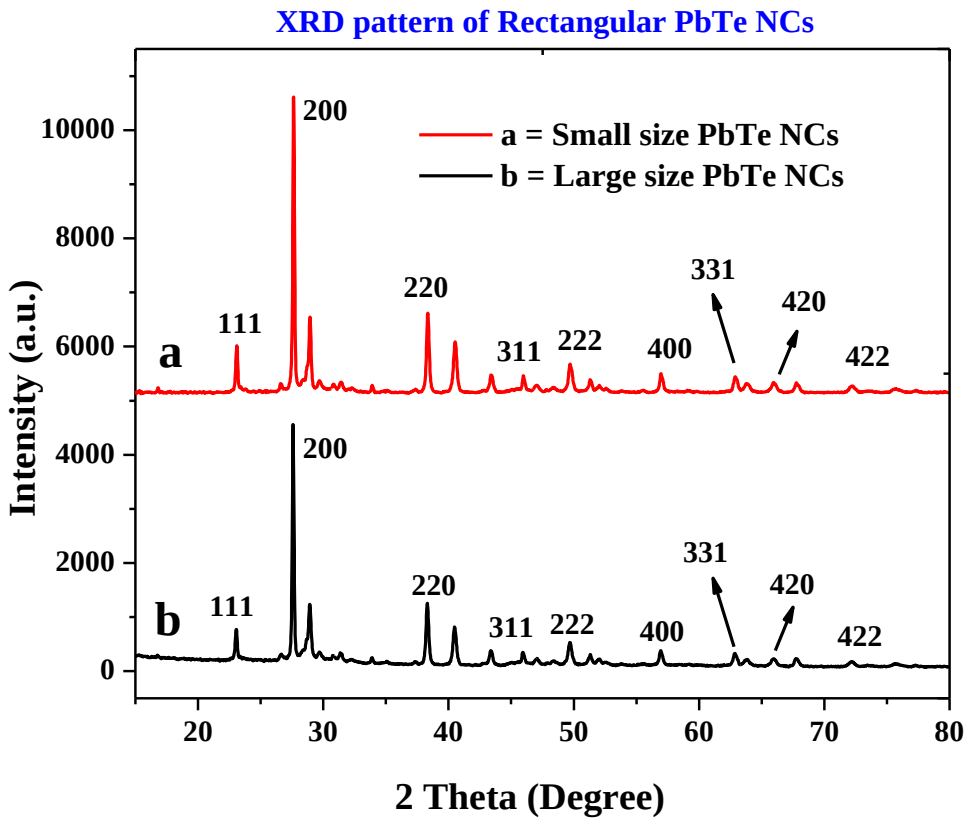

Figure 4

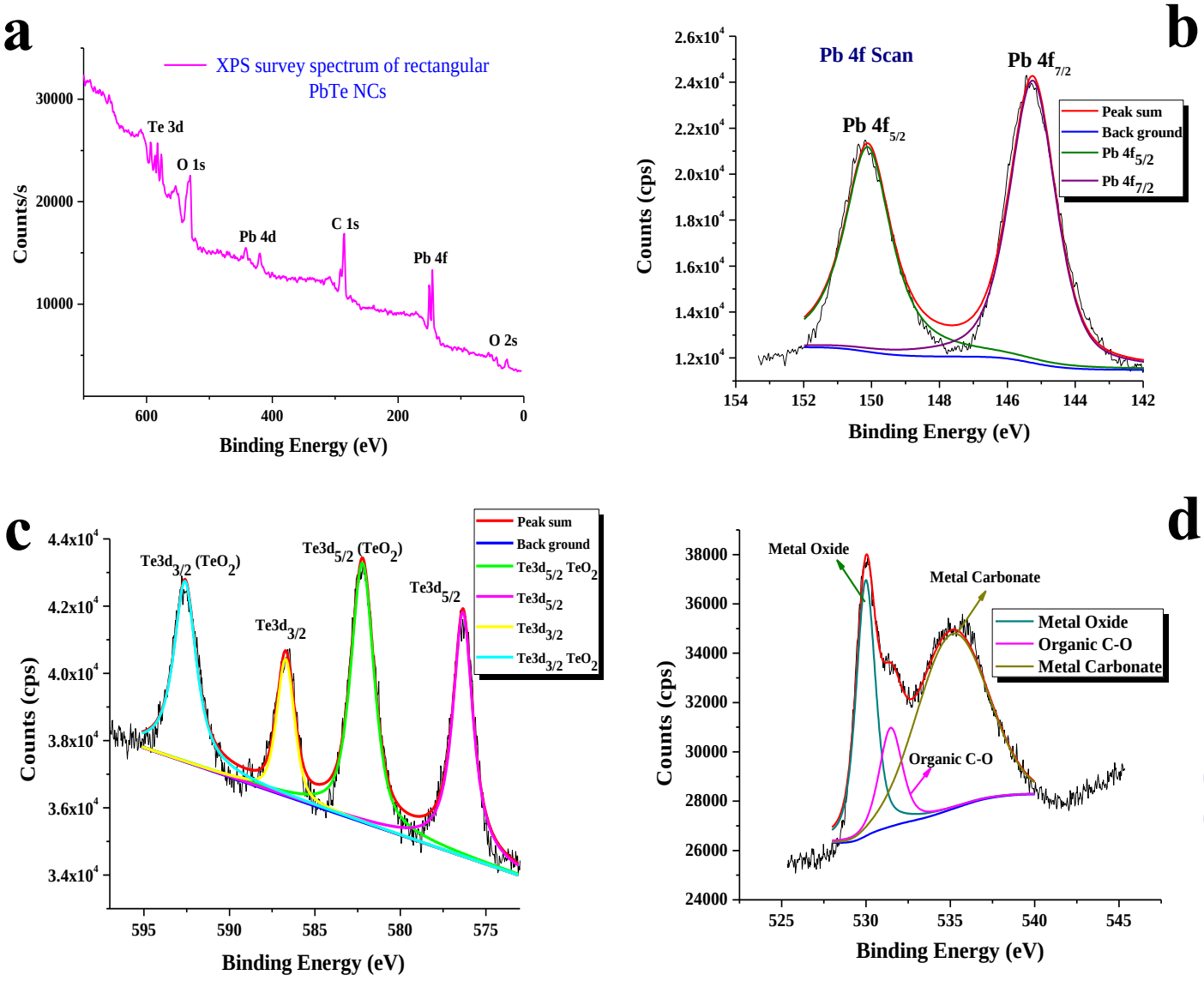

Figure 5, a-d

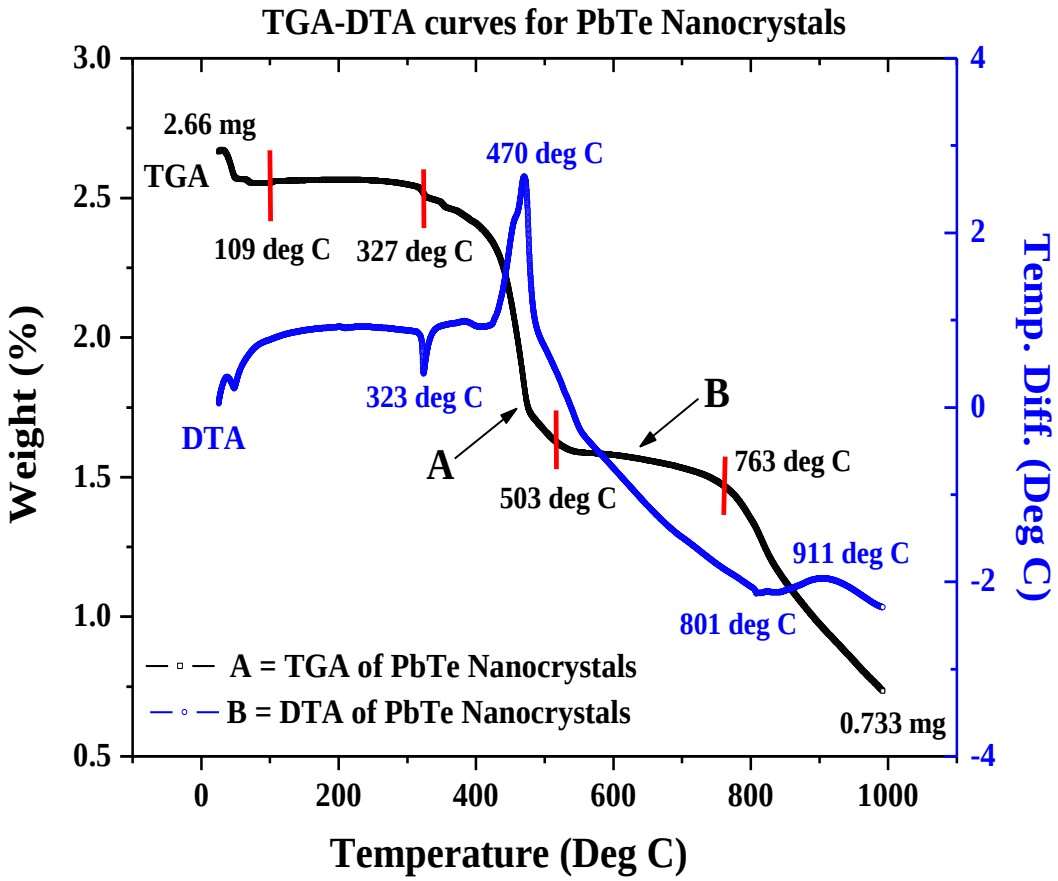

Figure 6

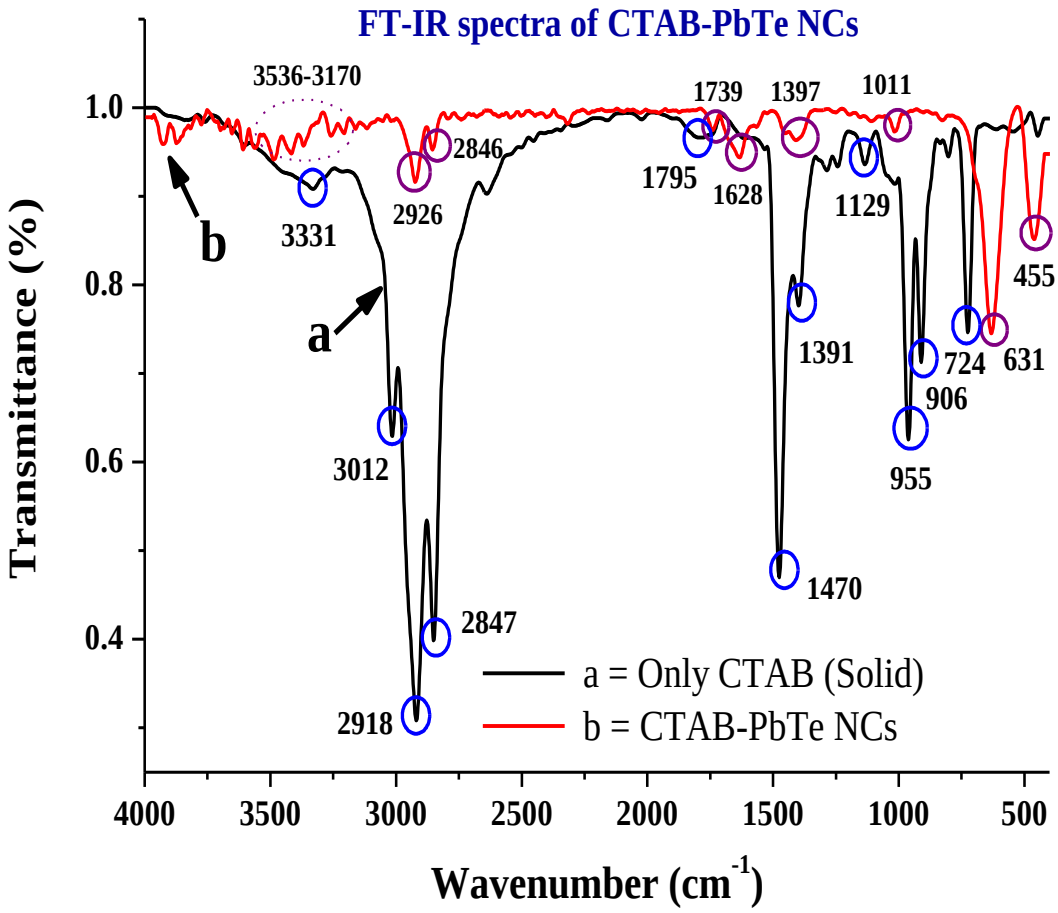

Figure 7

A

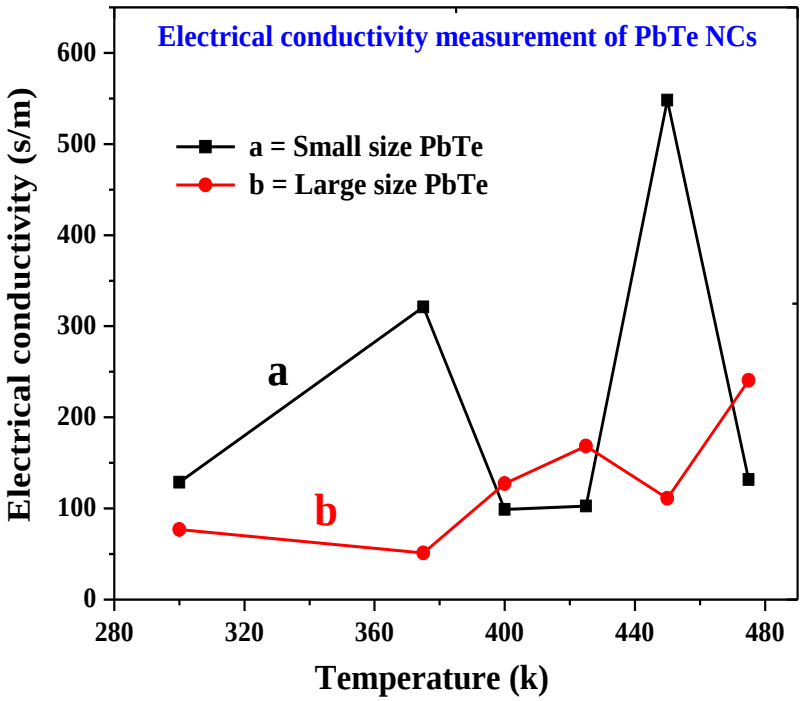

B

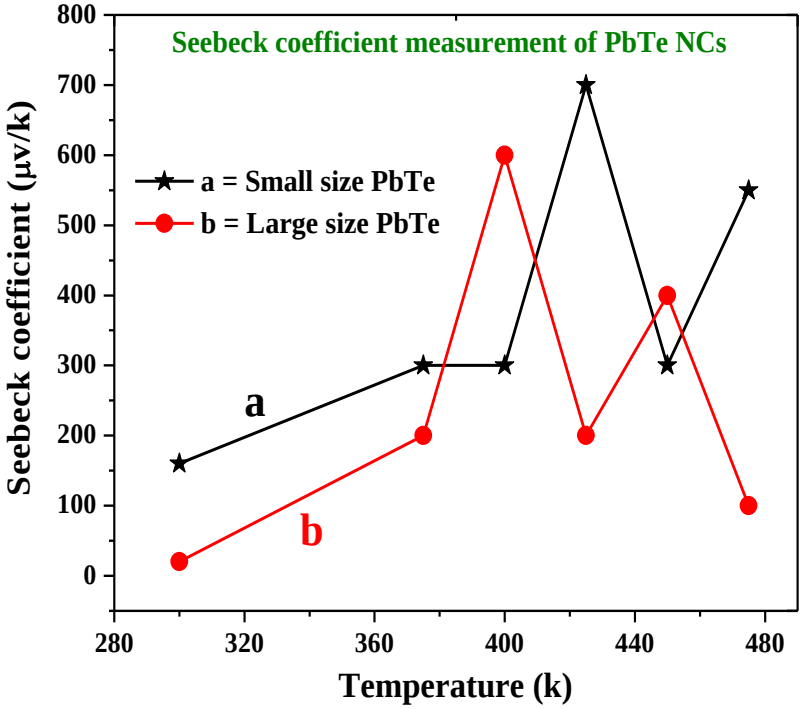

Figure 8, A-B

A

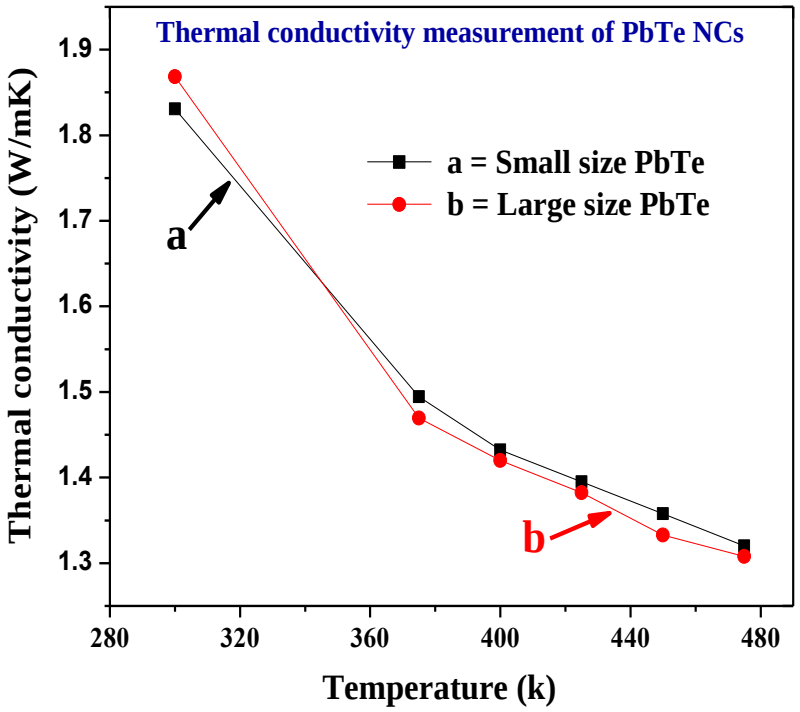

B

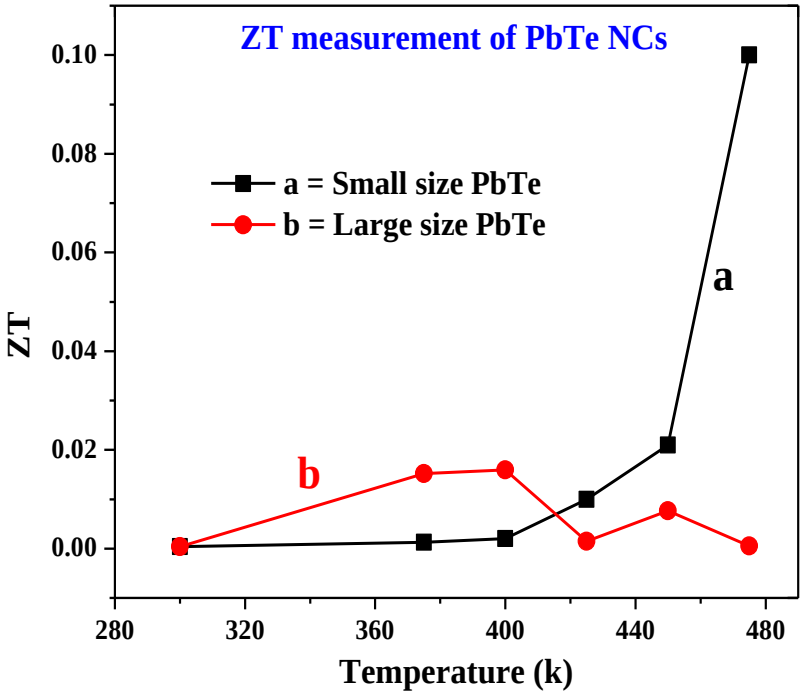

Figure 9, A-B

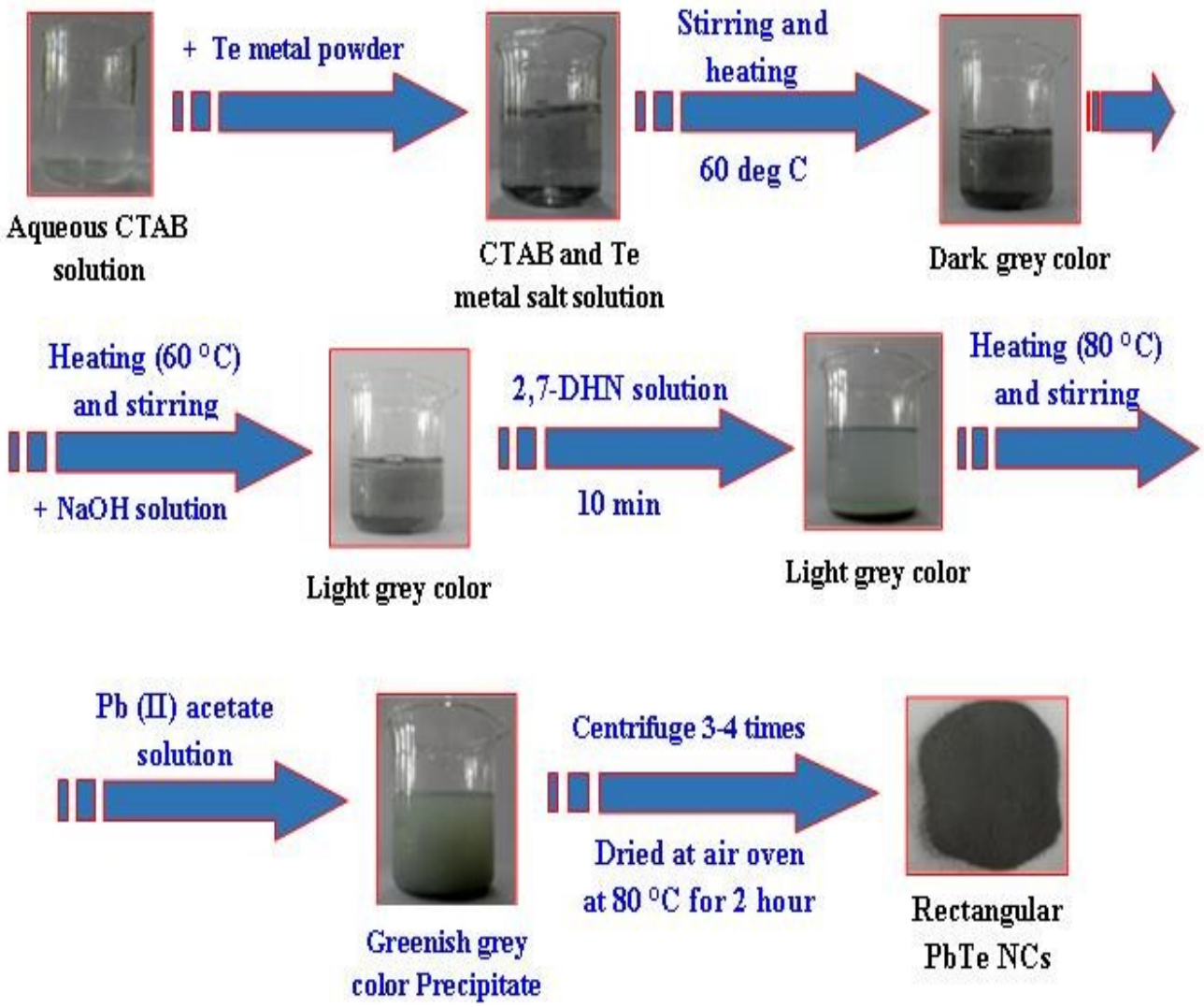

Scheme 1

Table 1

Set No.	Final conc. of CTAB (M)	Final conc. of Pb(II) Acetate solution (M)	Amount of Te metal powder (gm)	Final conc. of 2,7-DHN (M)	Final conc. of NaOH (M)	Color of the solution	Average particles size (nm)
1	7.6×10^{-5}	1.53×10^{-2}	0.6	5.12×10^{-3}	1.53	Light grey color	Side length 390 ± 20 nm, 230 ± 10 nm.
2	7.6×10^{-3}	1.53×10^{-2}	0.6	5.12×10^{-3}	1.53	Light grey color	Side length 260 ± 5 nm, 190 ± 20 nm.

Table 2

FT-IR bands – cetyl trimethyl ammonium bromide (CTAB)-Experimental and Reported values		
FT-IR bands (cm^{-1}) (experimentally observed)	**FT-IR frequency range (cm^{-1}) (reported value)**	**Absorbing bonds/vibration types**
3331	3330	–N-H stretching vibration
3012	2959, 2870	$-CH_3-$ anti-symmetrical and symmetrical stretching
2918, 2847	2916, 2828	$-(CH_2)-$ anti-symmetrical and symmetrical stretching
1391	1376	$-CH_3-$ symmetric deformation
1129, 1253, 1284	1300-1000 (1041,1151,1265)	$-(CH_2)-$ out-plane swinging
1034	1040	Symmetric stretching vibration C-N bonds
906, 955, 1470	908, 961, 1472	Tertiary Amine $[RN(CH_3)_3^+]$
724	720, 728	$-(CH_2)-$ in-plane swinging
Reference: Huang, L.; Chen, X.; Li, Q. *J. Mater. Chem.* **2001**, 11, 610.		

Table of Contents

Low Temperature Formation of Rectangular PbTe Nanocrystals and their Thermoelectric Applications

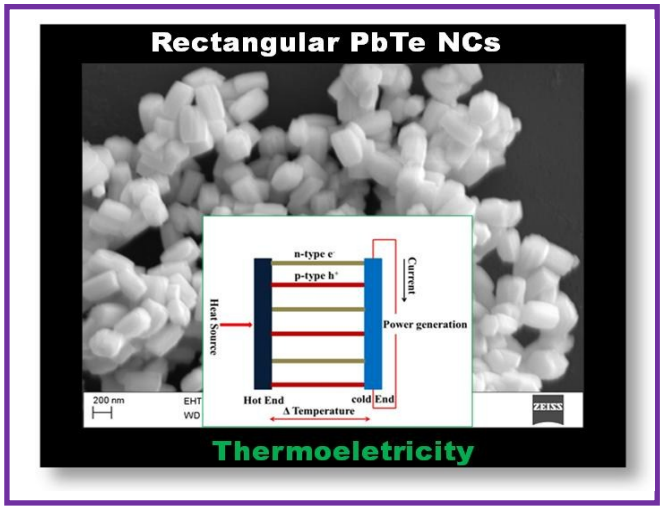

ABSTRACT

A low temperature route has been demonstrated for the generation of rectangular PbTe nanocrystals within short time which showed pronounced thermoelectric behavior.